Reproduction in whole or in part is permitted

for any purpose of the United States Government.

D D C

MAR 14 1978

F

DOUGLAS AIRCRAFT COMPANY

MCDONNELL DOUGLAS

CORPORATION

116 400

CALCULATION OF THREE-DIMENSIONAL BOUNDARY LAYERS ON

BODIES OF REVOLUTION AT INCIDENCE

by

Tuncer Cebeci, Richard S. Hirsh, and Kalle Kaups
Douglas Aircraft Company, Long Beach, California 90846

January 1978

FINAL REPORT

Copy number   Report number   MDC J7643

CALCULATION OF THREE-DIMENSIONAL BOUNDARY LAYERS
ON BODIES OF REVOLUTION AT INCIDENCE

Revision date   Revision letter

Issue date   January 1978   Contract number   N60921-76-C-0089

Prepared by :   Tuncer Cebeci, Richard S. Hirsh, Kalle Kaups

Approved by :

F. T. Lynch
Frank T. Lynch
Chief Aerodynamics Engineer
Research & Development

R. B. Harris
R. B. Harris
Chief Technology Engineer
Aerodynamics

DOUGLAS AIRCRAFT COMPANY

MCDONNELL DOUGLAS
CORPORATION

TABLE OF CONTENTS

LIST OF FIGURES

LIST OF SYMBOLS

A	Van Driest damping length
b	$1 + \varepsilon_m^+$
E	H/H_e
f	transformed vector potential for ψ
f'	u/u_e
g	transformed vector potential for ϕ
g'	w/u_e
h_1, h_2	metric coefficients of body
H	stagnation enthalpy
K_1, K_2, K_{11}, K_{12}	curvatures of body
L	modified mixing length
m_1, m_2, m_3, ...	coefficients in transformed equations
p	static pressure
Pr	Prandtl number
Pr_t	turbulent Prandtl number
Q	any general dependent variable
r	radius of body of revolution
R	Reynolds number
s_1	arc length along body
s_2	arc lenbth around body
t	axis ratio (thickness) of body of revolution
u, v, w	velocity components in x, y, θ directions
$\overline{u'v'}$, $\overline{w'v'}$, $\overline{v'H'}$	Reynolds stresses
u_τ	friction velocity
V	transformed normal velocity
x	coordinate down generator of body of revolution

y	coordinate normal to body of revolution
z	transformed azimuthal coordinate
α	angle of attack
$\epsilon_l, \epsilon_r, \epsilon_m, \epsilon_i, \epsilon_o$	eddy viscosities
η	transformed coordinate normal to surface
θ	azimuthal coordinate around body of revolution
μ	dynamic viscosity
ν	kinematic viscosity
ξ	transformed coordinate along body surface
ρ	density
ϕ, ψ	two component vector potential

Subscripts

e	edge values
w	wall values

primes denote differentiation with respect to η.

I. INTRODUCTION

In recent years, a number of methods have been developed in order to compute laminar and turbulent three-dimensional boundary layers. Although some are developed in a general way, most are developed to treat either of two specific classes of problems, i.e., flows on wings, or flows past bodies or revolution. Cebeci et al. [1] developed a general method for calculating the three-dimensional, compressible boundary layer on an arbitrary wing using the eddy-viscosity concept. Similar calculations have recently been presented by McLean [2] and by Kordulla [3]. Bradshaw et al. [4] simplified the three-dimensional equations on a swept tapered wing by assuming conical similarity, and used a higher order turbulence model to solve for the flow. The history of flows past bodies of revolution is more extensive, dating back to the first studies by Moore [5] dealing with flow past a cone. Further studies by Cooke [6], Boericke [7] and others integrated the conically similar quasi-two-dimensional equations around the cone. The spinning cone and its attendant problems were investigated by Dwyer [8] and Kitchens et al. [9]. The difficulties encountered in all the previous works due to behavior near the lee side of the cone, or crossflow reversal, were effectively overcome by Lin and Rubin [10], [11] who developed an augmented set of boundary-layer equations for treating problems of this kind.

The flow past a more general body of revolution, a prolate spheroid, has been extensively studied by Wang [12] - [14]. Although the cone is a special case of a general body of revolution, for the prolate spheroid at least, some of the more troublesome aspects of the cone flow do not appear. The nonexistence of solutions on the lee plane, found by Moore [5] and further investigated by Roux [15] and Murdock [16], does not seem to apply to the prolate spheroid. The crossflow separation, which causes the quasi-two-dimensional conical flow to experience a square-root singularity, does not seem to exert such an effect on the equations governing the prolate-spheroid flow. This has allowed Wang to carefully map the attached flow on the prolate spheroid at incidence by integrating from either the windward or leeward symmetry plane, something which cannot generally be done on a cone using standard boundary-layer procedures.

1

The general characteristics of the viscous flow past a body of revolution can be broadly described as follows. Depending on the incidence of the body, the flow can be thought to consist of three overlapping, and not-at-all distinct, regimes: (a) low incidence, where no separation occurs and three-dimensional boundary-layer theory applies; (b) low to moderate incidence, where the cross flow around the body separates and may possibly produce streamwise vortices which, however, still remain within the viscous layer; (c) higher incidences, where vortices detach from the body and alter the prevailing inviscid flow. Case (c) requires the complete (and possibly unsteady) Navier-Stokes equations, but case (b) can be described by a simpler set of equations called here the Parabolic-Elliptic Boundary-Layer (PEBL) equations.

Under the research sponsored by contract N60921-76-C-0089, aspects of this problem were investigated at Douglas during the past year, with the emphasis being towards the development of a general computer program for calculating the boundary layer on an arbitrary body of revolution using the classical three-dimensional boundary-layer equations, i.e., case (a). A parallel effort used the PEBL approach in order to extend the calculations to case (b). This report presents the results of the first phase of the above contract. Calculations were performed on a simple body of revolution, the prolate spheroid. For the case of the standard three-dimensional boundary-layer equations, the prolate spheroid produces a region of reverse crossflow, due to an adverse pressure gradient, but without a change of sign of the cross-flow edge velocity. Thus, the method used in [1], where the cross-flow integration direction is changed when the edge velocity changes sign, cannot be used, and the behavior of the finite-difference solution technique becomes apparent. The PEBL approach is used for the first time on a general body with variable metric coefficients (not simply a cone) and the sensitivity of the procedure to streamwise separation can be assessed.

A supplementary effort dealt with the incorporation of a new scaling law into the quasi-two-dimensional conical boundary-layer equations for the turbulent flow on a cone [17]. A suggestion made by Bradshaw [4], concerning the choice of similarity variable to be used in the computation, was followed, and produced noticeably better comparisons with the experimental data. These, and other results from the various programs will be described in the succeeding sections.

II. GOVERNING EQUATIONS

2.1 The Boundary-Layer Equations for a General Body of Revolution

In this report we consider the solution of more general three-dimensional boundary-layer equations than those discussed in our previous studies [1],[18], [19]. The generalization is due to the inclusion of crossflow diffusion terms. A detailed derivation is given in Appendix A. These generalized equations allow for the computation of negative crossflow due to the elliptic nature of the equations in crossflow plane. By using numerical schemes such as ADI (alternating-direction-implicit) procedures, they provide a means of comparing solutions with those obtained from standard boundary-layer procedures such as the Box scheme used in the present study as well as in our previous studies. For three-dimensional incompressible flows in a curvilinear orthogonal coordinate system, these generalized equations, which for brevity we shall refer to as PEBL (parabolic-elliptic boundary-layer) equations, are given by

Continuity

$$\frac{\partial}{\partial x}(h_2 u) + \frac{\partial}{\partial \theta}(h_1 w) + \frac{\partial}{\partial y}(h_1 h_2 v) = 0 \qquad (2.1.1)$$

x-Momentum

$$\frac{u}{h_1}\frac{\partial u}{\partial x} + \frac{w}{h_2}\frac{\partial u}{\partial \theta} + v\frac{\partial u}{\partial y} - uwK_1 + w^2 K_2 = -\frac{1}{\rho h_1}\frac{\partial p}{\partial x} + \frac{\partial}{\partial y}\left(\nu\frac{\partial u}{\partial y} - \overline{u'v'}\right)$$

$$+ \frac{1}{h_2}\frac{\partial}{\partial \theta}\left(\nu\frac{1}{h_2}\frac{\partial u}{\partial \theta} - \overline{u'w'}\right) \qquad (2.1.2)$$

θ-Momentum

$$\frac{u}{h_1}\frac{\partial w}{\partial x} + \frac{w}{h_2}\frac{\partial w}{\partial \theta} + v\frac{\partial w}{\partial y} - uwK_2 + u^2 K_1 = -\frac{1}{\rho h_2}\frac{\partial p}{\partial \theta} + \frac{\partial}{\partial y}\left(\nu\frac{\partial w}{\partial y} - \overline{w'v'}\right)$$

$$+ \frac{1}{h_2}\frac{\partial}{\partial \theta}\left(\nu\frac{1}{h_2}\frac{\partial w}{\partial \theta} - \overline{w'^2}\right)$$

$$- 2\nu\frac{1}{h_2}K_2\frac{\partial u}{\partial \theta} \qquad (2.1.3)$$

Note that if the underlined terms in (2.1.2) and (2.1.3) are set equal to zero, we recover the usual three-dimensional boundary-layer equations which we shall

3

refer to as the standard three-dimensional boundary-layer equations. In the above equations h_1 and h_2 are metric coefficients and are functions of x and θ, that is,

$$h_1 = h_1(x,\theta) \quad , \quad h_2 = h_2(x,\theta) \tag{2.1.4a}$$

The parameters K_1 and K_2 are known as the geodesic curvatures of the curves $\theta = $ const. and $x = $ const., respectively. They are given by

$$K_1 = -\frac{1}{h_1 h_2}\frac{\partial h_1}{\partial \theta} \quad , \quad K_2 = -\frac{1}{h_1 h_2}\frac{\partial h_2}{\partial x} \tag{2.1.4b}$$

At the edge of the boundary layer, (2.1.2) and (2.1.3) reduce to

$$\frac{u_e}{h_1}\frac{\partial u_e}{\partial x} + \frac{w_e}{h_2}\frac{\partial u_e}{\partial \theta} - u_e w_e K_1 + w_e^2 K_2 = -\frac{1}{\rho h_1}\frac{\partial p}{\partial x} + \frac{1}{h_2}\frac{\partial}{\partial \theta}\left(\nu \frac{1}{h_2}\frac{\partial u_e}{\partial \theta}\right) \tag{2.1.5a}$$

$$\frac{u_e}{h_1}\frac{\partial w_e}{\partial x} + \frac{w_e}{h_2}\frac{\partial w_e}{\partial \theta} - u_e w_e K_2 + u_e^2 K_1 = -\frac{1}{\rho h_2}\frac{\partial p}{\partial \theta} + \frac{1}{h_2}\frac{\partial}{\partial \theta}\left(\nu \frac{1}{h_2}\frac{\partial w_e}{\partial \theta}\right) - 2\nu \frac{1}{h_2} K_2 \frac{\partial u_e}{\partial \theta}$$

$$\tag{2.1.5b}$$

The solution of the system (2.1.1) - (2.1.4) requires both closure assumptions for the Reynolds stresses, and appropriate boundary conditions. The closure model will be discussed in Section 2.4. Some of the boundary conditions which need to be applied depend upon whether the standard or PEBL equations are to be solved. In either case, however, edge and wall boundary conditions for zero mass transfer are:

$$y = 0 \qquad\qquad u,w = 0 \qquad\qquad v = 0 \tag{2.1.6a}$$

$$y \rightarrow \infty \qquad\qquad u \rightarrow u_e(x,\theta) \qquad\qquad w \rightarrow w_e(x,\theta) \tag{2.1.6b}$$

The standard boundary-layer equations also require starting solutions on two intersecting planes. One of these is the windward plane of symmetry of the body. The other is chosen as the line $x = $ constant around the nose of the body where the value of x is equal to the value of x at the stagnation point. On this line the assumption is made that the flow behaves as if it were along an azimuthal attachment line. This eliminates the need to trace streamlines from the stagnation point around the nose of the body. Since for all the bodies considered in this report the stagnation line is extremely close to the

4

nose, the effect of this assumption is not felt after a few x steps downstream of the starting solution due to the parabolic nature of the boundary-layer equations.

On the windward plane of symmetry $w = 0$, but $w_\theta \neq 0$, and all other θ-derivatives are zero. The θ-momentum equation, (2.1.3) is singular on this line, but by differentiating it with respect to θ, a complete set of equations is obtained. Thus, the <u>windward symmetry plane</u> equations are:

Continuity

$$\frac{\partial}{\partial x} (h_2 u) + h_1 w_\theta + \frac{\partial}{\partial y} (h_1 h_2 v) = 0 \tag{2.1.7}$$

x-momentum

$$\frac{u}{h_1} \frac{\partial u}{\partial x} + v \frac{\partial u}{\partial y} = \frac{u_e}{h_1} \frac{\partial u_e}{\partial x} + \frac{\partial}{\partial y} \left(\frac{\partial u}{\partial y} - \overline{u'v'} \right) \tag{2.1.8}$$

θ-momentum

$$\frac{u}{h_1} \frac{\partial w_\theta}{\partial x} + \frac{1}{h_2} w_\theta^2 + v \frac{\partial w_\theta}{\partial y} - u w_\theta K_2 = \frac{u_e}{h_1} \frac{\partial w_{\theta e}}{\partial x} + \frac{1}{h_2} w_{\theta e}^2 - u_e w_{\theta e} K_2$$

$$+ \frac{\partial}{\partial y} \left[\nu \frac{\partial w_\theta}{\partial y} - (\overline{w'v'})_\theta \right] \tag{2.1.9}$$

Here $w_\theta = \partial w / \partial \theta$, $w_{\theta e} = \partial w_e / \partial \theta$. These equations are subject to the following boundary conditions

$$y = 0 \qquad u, w_\theta = 0 \qquad v = 0 \tag{2.1.10a}$$

$$y \to \infty \qquad u \to u_e(x) \qquad w_\theta \to w_{\theta e}(x) \tag{2.1.10b}$$

The equations on the azimuthal attachment line are very similar to the symmetry plane equations except that now the assumption is made that $u = 0$, $u_x \neq 0$, and all other x derivatives are zero. Note again that this is just an approximation. Now the x-momentum equation is singular but can be utilized after differentiation with respect to x. This yields the <u>azimuthal attachment line</u> equations:

Continuity

$$h_2 u_x + \frac{\partial}{\partial \theta} (h_1 w) + \frac{\partial}{\partial y} (h_1 h_2 v) = 0 \tag{2.1.11}$$

x-momentum

$$\frac{1}{h_1} u_x^2 + \frac{w}{h_2} \frac{\partial u_x}{\partial \theta} + v \frac{\partial u_x}{\partial y} - u_x w K_1 = \frac{1}{h_1} u_{xe}^2 + \frac{w}{h_2} \frac{\partial u_{xe}}{\partial \theta} - u_{xe} w_e K_1$$

$$+ \frac{\partial}{\partial y} \left[\nu \frac{\partial u_x}{\partial y} - (\overline{u'v'})_x \right] \qquad (2.1.12)$$

z-momentum

$$\frac{w}{h_2} \frac{\partial w}{\partial \theta} + v \frac{\partial w}{\partial y} = \frac{w_e}{h_2} \frac{\partial w_e}{\partial \theta} + \frac{\partial}{\partial y} \left(\nu \frac{\partial w}{\partial y} - \overline{w'v'} \right) \qquad (2.1.13)$$

Here $u_x = \partial u/\partial x$, $u_{xe} = \partial u_e/\partial x$ and the equations are subject to the boundary conditions

$$y = 0 \qquad\qquad u_x, w = 0 \qquad\qquad v = 0 \qquad\qquad (2.1.14a)$$

$$y \to \infty \qquad\qquad u_x \to u_x(\theta) \qquad\qquad w \to w(\theta) \qquad\qquad (2.1.14b)$$

The flow at the stagnation point itself is the first point calculated in the solution procedure. Here a combination of both attachment line and symmetry plane procedures is used to produce the equations for a general three-dimensional stagnation point boundary layer.

If the PEBL equations are to be solved, rather than the standard equations, it is necessary to prescribe conditions on two boundary surfaces of the azimuthal direction since equations (2.1.2) and (2.1.3) are elliptic in the θ coordinate. On a body of revolution, two symmetry planes exist on the windward and leeward generators. Thus, at both $\theta = 0$ and $\theta = \pi$ we have

$$u_\theta = 0 \qquad ; \qquad\qquad w = 0 \qquad\qquad (2.1.15)$$

It is not necessary to solve different symmetry plane equations, as is done in boundary-layer calculations, to start the calculation in the θ-direction. The equations (2.1.2) and (2.1.3) are simply solved in the entire θ-y-plane subject to the appropriate boundary conditions stated above. An initial data plane is also required, as in the standard case, for all the calculations to be made here using the PEBL equations. The standard equations are used to generate this solution, i.e., (2.1.11) - (2.1.14).

6

2.2 The Boundary Layer on a Conical Surface

If we are specifically interested in boundary layers on conical surfaces, then we have $h_1 = 1$ and $h_2 = x$. It follows from (2.1.4b) that $K_1 = 0$ and $K_2 = -1/x$. For compressible flow, the standard three-dimensional boundary-layer equations equivalent to (2.1.1) - (2.1.3) are:

Continuity:

$$\frac{\partial}{\partial x}(x\rho u) + \frac{\partial}{\partial \theta}(\rho w) + \frac{\partial}{\partial y}(x\overline{\rho v}) = 0 \tag{2.2.1}$$

x-Momentum:

$$\rho u \frac{\partial u}{\partial x} + \rho \frac{w}{x}\frac{\partial u}{\partial \theta} + \overline{\rho v}\frac{\partial u}{\partial y} - \rho\frac{w^2}{x} = \frac{\partial}{\partial y}\left(\mu\frac{\partial u}{\partial y} - \rho\overline{u'v'}\right) \tag{2.2.2}$$

θ-Momentum:

$$\rho u \frac{\partial w}{\partial x} + \rho \frac{w}{x}\frac{\partial w}{\partial \theta} + \overline{\rho v}\frac{\partial w}{\partial y} + \rho\frac{uw}{x} = -\frac{1}{x}\frac{dp}{d\theta} + \frac{\partial}{\partial y}\left(\mu\frac{\partial w}{\partial y} - \rho\overline{w'v'}\right) \tag{2.2.3}$$

Here θ denotes the polar coordinate in the developed plane; x the coordinate along the generators; and y the coordinate normal to the surface; with w, u, v the velocities in the θ, x, and y directions. The boundary conditions for these equations have already been given as (2.1.6a) and (2.1.6b).

In compressible flow it is also necessary to have the energy equation to close the system of equations. In the present notation it becomes:

Energy:
$$\rho u \frac{\partial H}{\partial x} + \rho \frac{w}{x}\frac{\partial H}{\partial \theta} + \overline{\rho v}\frac{\partial H}{\partial y} = \frac{\partial}{\partial y}\left[\frac{\mu}{Pr}\frac{\partial H}{\partial y} + \mu\left(1 - \frac{1}{Pr}\right)\frac{\partial}{\partial y}\left(\frac{u^2 + w^2}{2}\right) - \rho\overline{v'H'}\right]$$
$$\tag{2.2.4}$$

where H is the stagnation enthalpy, and Pr the Prandtl number. The boundary conditions on the enthalpy are

$y = 0$	H = given	or	$\partial H/\partial y$ = given	(2.2.5a)
$y \to \infty$	$H \to H_e(x,\theta)$			(2.2.5b)

At the windward stagnation line, $\theta = 0$, the cross-flow momentum equation is singular. Taking into account the symmetry conditions and differentiating (2.2.3) with respect to θ, we can write it as

7

$$\rho u \frac{\partial w_\theta}{\partial x} + \rho \frac{w_\theta^2}{x} + \overline{\rho v} \frac{\partial w_\theta}{\partial y} + \rho \frac{u w_\theta}{x} = -\frac{1}{x} \frac{d^2 p}{d\theta^2} + \frac{\partial}{\partial y} \left[\mu \frac{\partial w_\theta}{\partial y} - \rho (\overline{w'v'})_\theta \right] \quad (2.2.6)$$

Noting that $w = 0$, (2.2.1), (2.2.2) and (2.2.4) can be simplified and written as

$$\frac{\partial}{\partial x} (x\rho u) + \rho w_\theta + \frac{\partial}{\partial y} (x\overline{\rho v}) = 0 \quad (2.2.7)$$

$$\rho u \frac{\partial u}{\partial x} + \overline{\rho v} \frac{\partial u}{\partial y} = \frac{\partial}{\partial y} \left(\mu \frac{\partial u}{\partial y} - \rho \overline{u'v'} \right) \quad (2.2.8)$$

$$\rho u \frac{\partial H}{\partial x} \quad \overline{\rho v} \frac{\partial H}{\partial y} = \frac{\partial}{\partial y} \left[\frac{\mu}{Pr} \frac{\partial H}{\partial y} + \mu \left(1 - \frac{1}{Pr} \right) \frac{\partial}{\partial y} \left(\frac{u^2}{2} \right) - \rho \overline{v'H'} \right] \quad (2.2.9)$$

where $w_\theta = \partial w/\partial \theta$. The boundary conditions for this set of equations is given by (2.1.10a) and (2.1.10b) plus (2.2.5a) and

$$y \to \infty \qquad H \to H_e(x) \qquad (2.2.10)$$

2.3 Geometry and Coordinate System

Three-dimensional boundary layers develop, in general, on a nondevelopable surface. This means that the computations cannot be made on a Cartesian coordinate system; instead a curvilinear coordinate system must be used. There are several possible coordinate systems. One possibility is a streamline system. Here the external streamlines form one family of the coordinate lines, and the equipotential lines (orthogonal everywhere to the streamlines) form the other family of the coordinate lines. The use of this system enables the streamwise and crosswise velocity profiles to be computed easily and is one of the most popular coordinate systems used in integral methods. However, the determination of the streamline coordinate system requires a knowledge of the external flow in considerable detail. In addition, the numerical computation of the associated geometrical parameters is quite involved. As a result, when a differential approach such as ours is used, this coordinate system is not very attractive.

Another coordinate system, popular for bodies of revolution, is the one used by Blottner and Ellis [20]. Here the coordinate system is determined by the intersection with the body surface of parallel planes which pass through an axis containing the stagnation point. The other coordinate lines are

8

obtained numerically from the orthogonality condition. When this system is employed, the computations can start immediately from the stagnation point, pass through the nose of the body and march downstream to the separation point. Again this coordinate system requires a lot of numerical work to determine the computational and the geometrical parameters.

At small angles of attack the stagnation point is close to the nose of the body. A very attractive coordinate system is the body coordinate system, in which one coordinate, say θ, is formed by the lines $x = constant$, and the other coordinate, s, is the line $\theta = constant$ along the meridional direction, either measured along the surface or measured along the x-axis. For numerical work the latter is preferred. It is this body-oriented coordinate system which we shall use in the present work, see Section 5.1 for a specific example.

2.4 Closure Assumptions for the Reynolds Stresses

The solution of any of the sets of boundary-layer equations derived in Section 2.1 requires closure assumptions for the Reynolds shear stresses, $-\rho\overline{u'v'}$, $-\rho\overline{w'v'}$. As in our previous studies we use the eddy-viscosity concept and define

$$-\overline{u'v'} = \epsilon_1 \frac{\partial u}{\partial y} \qquad , \qquad -\overline{w'v'} = \epsilon_2 \frac{\partial w}{\partial y} \qquad (2.4.1)$$

Following the formulation of reference 19, we assume that $\epsilon_1 = \epsilon_2 = \epsilon_m$ and define ϵ_m by two separate formulas. In the so-called inner region of the boundary layer, ϵ_m is defined by

$$\epsilon_m = \epsilon_i = L^2 \left[\left(\frac{\partial u}{\partial y} \right)^2 + \left(\frac{\partial w}{\partial y} \right)^2 \right]^{1/2} = L^2 S(y) \qquad (2.4.2)$$

where

$$L = 0.4y[1 - \exp(-y/A)], \quad s(y) = \left[\left(\frac{\partial u}{\partial y} \right)^2 + \left(\frac{\partial w}{\partial y} \right)^2 \right]^{1/2} \qquad (2.4.3a)$$

$$A = 26 \frac{\nu}{u_\tau} \qquad , \qquad u_\tau = (\nu S_w)^{1/2} \qquad (2.4.3b)$$

9

In the outer region ϵ_m is defined by

$$\epsilon_m = \epsilon_o = 0.0168 \left| \int_0^\infty (u_{te} - u_t)dy \right| \qquad (2.4.4)$$

where

$$u_{te} = (u_e^2 + w_e^2)^{1/2} \quad , \qquad u_t = (u^2 + w^2)^{1/2} \qquad (2.4.5)$$

where the inner and outer regions are established by the continuity of the eddy-viscosity formula.

III. TRANSFORMATION OF THE GOVERNING EQUATIONS

3.1 Transformation of the Standard Boundary-Layer Equations

The boundary-layer equations can be solved when they are expressed either in physical coordinates or in transformed coordinates. Each coordinate system has its own advantages. In problems where computer storage becomes important, the choice of using transformed coordinates becomes necessary, as well as convenient, since the transformed coordinates allow large steps to be taken in the x and θ directions. The reason for this is that the profiles expressed in the transformed coordinates do not change as rapidly as they do when they are expressed in physical coordinates. The use of transformed coordinates also stretches the coordinate normal to the wall and takes out much of the variation in boundary-layer thickness for laminar flows. Since the standard and parabolic-elliptic equations will be solved by different methods, and because there are additional terms in PEBL, the transformation of each set will be considered separately.

For the standard equations, we first define the transformed coordinates by

$$x = x \quad , \quad z = \theta \quad , \quad d\eta = \left(\frac{u_e}{\nu s_1}\right)^{1/2} dy \qquad (3.1.1)$$

and introduce a two-component vector potential such that

$$h_2 u = \frac{\partial \psi}{\partial y} \quad , \quad h_1 w = \frac{\partial \phi}{\partial y} \quad , \quad h_1 h_2 v = -\left(\frac{\partial \psi}{\partial x} + \frac{\partial \phi}{\partial z}\right) \qquad (3.1.2)$$

In addition, we define dimensionless f and g related to ψ and ϕ by

$$\psi = (u_e \nu s_1)^{1/2} h_2 \, f(x,z,\eta) \qquad (3.1.3a)$$

$$\phi = (u_e \nu s_1)^{1/2} h_1 \frac{w_e}{u_e} g(x,z,\eta) \qquad (3.1.3b)$$

Here s_1, which denotes the arc length along the x-coordinate, is defined by

$$s_1 = \int_{-1}^{x} h_1 \, dx \qquad (3.1.4)$$

11

Introducing the expressions (3.1.1) to (3.1.4) into (2.1.2) and (2.1.3) for the standard equations, we get after considerable algebra,

x-momentum

$$(bf'')' + m_1 ff'' - m_2(f')^2 - m_5 f'g' + m_6 f''g - m_8(g')^2 + m_{11}$$

$$= m_{10}\left(f'\frac{\partial f'}{\partial x} - f''\frac{\partial f}{\partial x}\right) + m_7\left(g'\frac{\partial f'}{\partial z} - f''\frac{\partial g}{\partial z}\right) \qquad (3.1.5)$$

z-momentum

$$(bg'')' + m_1 fg'' - m_3(g')^2 - m_4 f'g' + m_6 gg'' - m_9(f')^2 + m_{12}$$

$$= m_{10}\left(f'\frac{\partial g'}{\partial x} - g''\frac{\partial f}{\partial x}\right) + m_7\left(g'\frac{\partial g'}{\partial z} - g''\frac{\partial g}{\partial z}\right) \qquad (3.1.6)$$

Here primes denote differentiation with respect to η and

$$f' = \frac{u}{u_e} \qquad g' = \frac{w}{u_e} \qquad b = 1 + \epsilon_m^+ \qquad \epsilon_m^+ = \frac{\epsilon_m}{\nu} \qquad (3.1.7)$$

The coefficients m_1 to m_{12} are given by

$$m_1 = \frac{1}{2}\left(1 + \frac{S_1}{u_e h_1}\frac{\partial u_e}{\partial x} - 2S_1 K_2\right) \qquad m_2 = \frac{S_1}{u_e h_1}\frac{\partial u_e}{\partial x} \qquad m_3 = \frac{S_1}{u_e h_2}\frac{\partial w_e}{\partial z}$$

$$m_4 = \frac{S_1}{u_e h_1}\frac{\partial w_e}{\partial x} - K_2 S_1 \qquad m_5 = \frac{w_e}{u_e}\frac{S_1}{u_e h_2}\frac{\partial u_e}{\partial z} - K_1 S_1$$

$$m_6 = \frac{w_e}{u_e}\frac{S_1}{w_e h_2}\frac{\partial w_e}{\partial z} - \frac{S_1}{2u_e h_2}\frac{\partial u_e}{\partial z} - S_1 K_1 \qquad m_7 = \frac{S_1}{h_2}\frac{w_e}{u_e}$$

$$m_8 = \left(\frac{w_e}{u_e}\right)^2 K_2 S_1 \qquad m_9 = \frac{u_e}{w_e} K_1 S_1 \qquad (3.1.8)$$

$$m_{10} = \frac{S_1}{h_1} \qquad m_{11} = m_2 + m_5 + m_8 \qquad m_{12} = m_4 + m_3 + m_9$$

To transform the symmetry plane equations (2.1.7) - (2.1.9), we use relations (3.1.1) and (3.1.4) for the coordinates, with the dependent variables defined as

12

$$h_2 u = \frac{\partial \psi}{\partial y} \qquad\qquad h_1 w_z = \frac{\partial \phi}{\partial y} \qquad\qquad h_1 h_2 v = -\left(\frac{\partial \psi}{\partial x} + \phi\right) \qquad (3.1.9)$$

The dimensionless f and g are defined by

$$\psi = (u_e \nu S_1)^{1/2} h_2 f(x, \eta) \qquad (3.1.10a)$$

$$\phi = (u_e \nu S_1)^{1/2} h_1 \frac{w_{ze}}{u_e} g(x, \eta) \qquad (3.1.10b)$$

Using these variables the symmetry plane equations become

$$(bf'')' + m_1 ff'' - m_2 (f')^2 + m_6 f'' g + m_{11} = m_{10} \left(f' \frac{\partial f'}{\partial x} - f'' \frac{\partial f}{\partial x} \right) \qquad (3.1.11)$$

$$(bg'')' + m_1 fg'' - m_3 (g')^2 - m_4 f'g' + m_6 gg'' + m_{12} = m_{10} \left(f' \frac{\partial g'}{\partial x} - g'' \frac{\partial f}{\partial x} \right)$$

$$(3.1.12)$$

where

$$m_1 = \frac{1}{2}\left(1 + \frac{S_1}{u_e h_1}\frac{\partial u_e}{\partial x} - 2S_1 K_2\right) \qquad m_2 = \frac{S_1}{u_e h_1}\frac{\partial w_e}{\partial z} \qquad m_3 = \frac{S_1}{u_e h_2}\frac{\partial w_e}{\partial z}$$

$$m_4 = \frac{S_1}{w_{ze} h_1}\frac{\partial w_{ze}}{\partial x} - S_1 K_2 \qquad\qquad m_6 = m_3 \qquad\qquad m_{10} = \frac{S_1}{h_1}$$

$$m_{11} = m_2 \qquad\qquad\qquad\qquad m_{12} = m_3 + m_4 \qquad (3.1.13)$$

In the same manner, the attachment line equations (2.1.11) - (2.1.13) can be transformed by using

$$x = x \qquad\qquad z = \theta \qquad\qquad d\eta = \left(\frac{u_{xe}}{\nu h_1}\right)^{1/2} dy \qquad (3.1.14)$$

$$h_2 u_x = \frac{\partial \psi}{\partial y} \qquad\qquad h_1 w = \frac{\partial \phi}{\partial y} \qquad\qquad h_1 h_2 v = -\left(\psi + \frac{\partial \phi}{\partial z}\right) \qquad (3.1.15)$$

and

$$\psi = (u_{xe} \nu h_1)^{1/2} h_2 f(z, \eta) \qquad (3.1.16a)$$

$$\phi = (u_{xe} \nu h_1)^{1/2} h_1 \frac{w_e}{u_{xe}} g(z, \eta) \qquad (3.1.16b)$$

13

With these variables, the attachment line equations are

$$(bf'')' + ff'' - f'^2 - m_5 f'g' + m_6 gf'' + m_{11} = m_7 \left(g' \frac{\partial f'}{\partial z} - f'' \frac{\partial g}{\partial z} \right)$$

$$(3.1.17)$$

$$(bg'')' + fg'' - m_3 g'^2 + m_6 gg'' + m_{12} = m_7 \left(q' \frac{\partial g'}{\partial z} - g'' \frac{\partial g}{\partial z} \right)$$

where

$$m_3 = \frac{h_1}{h_2} \frac{1}{u_{xe}} \frac{\partial w_e}{\partial z}$$

$$m_5 = h_1 \frac{w_e}{u_{xe}} \left(\frac{1}{u_e h_2} \frac{\partial u_{xe}}{\partial z} - K_1 \right)$$

$$m_6 = (u_{xe} h_1)^{-1/2} \frac{1}{h_2} \frac{\partial}{\partial z} (h_1^{3/2} u_{xe}^{-1/2} w_e)$$

$$(3.1.18)$$

$$m_7 = \frac{h_1}{h_2} \frac{w_e}{u_{xe}}$$

$$m_{11} = 1 + m_5$$

$$m_{12} = m_3$$

The general boundary conditions which apply to the three-dimensional boundary-layer equations are

$$\eta = 0 \qquad\qquad f_w = f'_w = g_w = g'_w = 0 \qquad\qquad (3.1.19a)$$

$$\eta = \eta_\infty \qquad\qquad f' = 1, \quad g' = 1 \qquad\qquad (3.1.19b)$$

3.2 Transformation of the Conical Boundary-Layer Equations

It is well known that for laminar flows with nonporous walls and wall temperatures independent of x, or adiabatic wall conditions, the equations (2.2.1) to (2.2.4) have similarity solutions (i.e., solutions independent of x) if we define the similarity variable η by

$$d\eta = \left(\frac{u_e}{\rho_e \mu_e x} \right)^{1/2} \rho dy \qquad\qquad (3.2.1)$$

In addition, if we introduce a two-component vector potential such that

14

$$\rho ux = \frac{\partial \psi}{\partial y} \quad , \quad \rho wx = \frac{\partial \phi}{\partial y} \quad , \quad \overline{\rho v}x = -\frac{\partial \psi}{\partial x} - \frac{1}{x}\frac{\partial \phi}{\partial \theta} \quad (3.2.2)$$

and dimensionless functions ψ and ϕ by

$$\psi = (\rho_e \mu_e u_e)^{1/2} x^{3/2} f(\theta,\eta) \quad , \quad \phi = (\rho_e \mu_e u_e)^{1/2} x^{3/2} \frac{w_e}{u_e} g(\theta,\eta) \quad (3.2.3)$$

then it can be shown that the two momentum equations, (2.2.2) and (2.2.3), and the energy equation (2.2.4) can be written as

$$(bf'')' + \frac{3}{2} ff'' + m_1 gf'' + m_2^2 [(g')^2 - f'g'] = m_2 \left(g' \frac{\partial f'}{\partial \theta} - f'' \frac{\partial g}{\partial \theta} \right) \quad (3.2.4)$$

$$(bg'')' + \frac{3}{2} fg'' + m_1 gg'' + m_3 \left[\frac{\rho_e}{\rho} - (g')^2 \right] + \frac{\rho_e}{\rho} - f'g'$$

$$= m_2 \left(g' \frac{\partial g'}{\partial \theta} - g'' \frac{\partial g}{\partial \theta} \right) \quad (3.2.5)$$

$$\left[\frac{C}{Pr} \left(1 + \sqrt{2}\, \epsilon_m^+ \frac{Pr}{Pr_t} \right) E' + \frac{Cu_e^2}{H_e} \left(1 - \frac{1}{Pr} \right) (f'f'' + m_2^2 g'g'') \right]' + \frac{3}{2} fE' + m_1 gE'$$

$$= m_2 \left(g' \frac{\partial E}{\partial \theta} - E' \frac{\partial g}{\partial \theta} \right) \quad (3.2.6)$$

where primes denote differentiation with respect to η.

The definitions of the terms in (3.2.4) to (3.2.6) are:

$$f' = \frac{u}{u_e} \quad , \quad g' = \frac{w}{w_e} \quad , \quad E = \frac{H}{H_e} \quad , \quad b = C(1 + \epsilon_m^+) \quad , \quad \epsilon_m^+ = \frac{\epsilon_m}{\nu}$$

$$C = \frac{\rho \mu}{\rho_e \mu_e} \quad , \quad m_1 = m_3 - \frac{m_2^2}{2} + \frac{1}{2} \frac{m_2}{\rho_e \mu_e} \frac{d}{d\theta} (\rho_e \mu_e) \quad , \quad m_2 = \frac{w_e}{u_e} \quad ,$$

$$m_3 = \frac{1}{u_e} \frac{dw_e}{d\theta} \quad (3.2.7)$$

Here we have used the eddy viscosity and turbulent Prandtl number concepts and have written the turbulence terms by

$$-\rho \overline{u'v'} = \rho \epsilon_m \frac{\partial u}{\partial y} \qquad \qquad -\rho \overline{w'v'} = \rho \epsilon_m \frac{\partial w}{\partial y} \quad (3.2.8a)$$

$$-\rho \overline{v'H'} = \sqrt{2} \frac{\epsilon_m}{Pr_t} \frac{\partial H}{\partial y} \quad (3.2.8b)$$

15

Similarly, equations (2.2.6) to (2.2.9) can be transformed and expressed in a form similar to those given by (3.2.4) to (3.2.6) by using the transformations given by (3.2.1) to (3.2.3) with slight modification to the following parameters,

$$\rho w_\theta = \frac{\partial \theta}{\partial y} \qquad\qquad \overline{\rho v x} = -\frac{\partial \psi}{\partial x} - \phi \qquad (3.2.9)$$

$$\psi = (\rho_e \mu_e u_e)^{1/2} x^{3/2} f(\eta) \qquad\qquad \phi = (\rho_e \mu_e u_e x)^{1/2} \frac{(w_e)_\theta}{u_e} g(\eta) \qquad (3.2.10)$$

Equations (2.2.6) to (2.2.9) then become

$$(bf'')' + \frac{3}{2} ff'' + m_3 gf'' = 0 \qquad (3.2.11)$$

$$(bg'')' + \frac{3}{2} fg'' + m_3 gg'' + m_3 \left[\frac{\rho_e}{\rho} - (g')^2\right] + \frac{\rho_e}{\rho} - f'g' = 0 \qquad (3.2.12)$$

$$\left[\frac{C}{Pr}\left(1 + \sqrt{2}\,\varepsilon_m^+ \frac{Pr}{Pr_t}\right) E' + \frac{Cu_e^2}{H_e}\left(1 - \frac{1}{Pr}\right) ff''\right]' + \frac{3}{2} fE' + m_3 gE' = 0 \qquad (3.2.13)$$

Here

$$g' = \frac{w_\theta}{(w_e)_\theta}$$

The boundary conditions which are valid for either (3.2.4) - (3.2.6) or (3.2.11) - (3.2.13) are

$$\eta = 0 \qquad f = g = f' = g' = 0 \qquad E'_w \text{ or } E_w \text{ given} \qquad (3.2.14a)$$

$$\eta = \eta_\infty \qquad f' = g' = E = 1 \qquad (3.2.14b)$$

The usual procedure that has been followed in predicting the boundary-layer development on cones at incidence is to solve the system of equations given by (3.2.11) to (3.2.13) for $\theta = 0$, and (3.2.4) to (3.2.6) for $\theta > 0$ for both laminar and turbulent flows with a mixing-length or eddy-viscosity formulation. In those calculations it is assumed that the square-root variation of boundary-layer thickness for laminar flows also applies for turbulent flows.

16

Now, however, we do not follow this procedure for turbulent flows; instead we follow a recent suggestion of Bradshaw et al. [4] and assume that the velocity profiles u/u_e and w/w_e are similar if we define $Y = y/x$, rather than $y/\sqrt{x}$. It follows then that for any quantity q

$$\left(\frac{\partial q}{\partial x}\right)_y = \left(\frac{\partial q}{\partial x}\right)_Y + \left(\frac{\partial q}{\partial Y}\right)_x \frac{\partial Y}{\partial x} \tag{3.2.15a}$$

$$\left(\frac{\partial q}{\partial y}\right)_x = \left(\frac{\partial q}{\partial Y}\right)_x \frac{\partial Y}{\partial y} \tag{3.2.15b}$$

To have similarity $(\partial q/\partial x)_Y = 0$; then noting that $\partial Y/\partial x = -y/x^2$ and $\partial Y/\partial y = 1/x$, from (3.2.15), we can write

$$\frac{(\partial q/\partial x)_y}{(\partial q/\partial y)_x} = \frac{(\partial q/\partial Y)_x (\partial Y/\partial x)}{(\partial q/\partial Y)_x (\partial Y/\partial y)} = -\frac{y}{x} \tag{3.2.16}$$

so that

$$\frac{\partial q}{\partial x} = -\frac{y}{x} \frac{\partial q}{\partial y} \tag{3.2.17}$$

With this assumption, it can be shown that equations (3.2.1) to (3.2.4) can be written as

$$\frac{\partial}{\partial \theta}(\rho w) + \frac{\partial}{\partial y}(x\rho \hat{v}) + 2\rho u = 0 \tag{3.2.18}$$

$$\rho \frac{w}{x} \frac{\partial u}{\partial \theta} + \rho \hat{v} \frac{\partial u}{\partial y} - \rho \frac{w^2}{x} = \frac{\partial}{\partial y}\left(\mu \frac{\partial u}{\partial y} - \rho \overline{u'v'}\right) \tag{3.2.19}$$

$$\rho \frac{w}{x} \frac{\partial w}{\partial \theta} + \rho \hat{v} \frac{\partial w}{\partial y} + \rho \frac{uw}{x} = -\frac{1}{x} \frac{dp}{d\theta} + \frac{\partial}{\partial y}\left(\mu \frac{\partial w}{\partial y} - \rho \overline{w'v'}\right) \tag{3.2.20}$$

$$\rho \frac{w}{x} \frac{\partial H}{\partial \theta} + \rho \hat{v} \frac{\partial H}{\partial y} = \frac{\partial}{\partial y}\left[\frac{\mu}{Pr} \frac{\partial H}{\partial y} + \mu\left(1 - \frac{1}{Pr}\right)\frac{\partial}{\partial y}\left(\frac{u^2 + w^2}{2}\right) - \rho \overline{v'H'}\right] \tag{3.2.21}$$

where

$$\hat{v} = \frac{\overline{\rho v}}{\rho} - u \frac{y}{x} \tag{3.2.22}$$

Similarly, the windward stagnation-line equations can be written as

$$\rho w_\theta + \frac{\partial}{\partial y} x\rho \hat{v} + 2\rho u = 0 \tag{3.2.23}$$

$$\rho \hat{v} \frac{\partial u}{\partial y} = \frac{\partial}{\partial y}\left(\mu \frac{\partial u}{\partial y} - \rho \overline{u'v'}\right) \tag{3.2.24}$$

17

$$\rho \hat{v} \frac{\partial w_\theta}{\partial y} + \rho \frac{w_\theta^2}{x} + \rho \frac{uw_\theta}{x} = -\frac{1}{x} \frac{d^2 p}{d\theta^2} + \frac{\partial}{\partial y} \left[\mu \frac{\partial w_\theta}{\partial y} - \rho (\overline{w'v'})_\theta \right] \qquad (3.2.25)$$

$$\rho \hat{v} \frac{\partial H}{\partial y} = \frac{\partial}{\partial y} \left[\frac{\mu}{Pr} \frac{\partial H}{\partial y} + \mu \left(1 - \frac{1}{Pr}\right) \frac{\partial}{\partial y} \left(\frac{u^2}{2}\right) - \rho \overline{v'H'} \right] \qquad (3.2.26)$$

If we now apply the transformation given by (3.2.1) to (3.2.3) with $\rho \hat{v} x$ defined by

$$\rho \hat{v} x = -2 \frac{\psi}{x} - \frac{1}{x} \frac{\partial \phi}{\partial \theta} \qquad (3.2.27)$$

to (3.2.18) to (3.2.21) and the transformation given by (3.2.9), (3.2.10) with $\rho \hat{v} x$ defined by

$$\rho \hat{v} x = -2 \frac{\psi}{x} - \frac{\phi}{x} \qquad (3.2.28)$$

to (3.2.23) to (3.2.26), it can be shown that the resulting transformed equations are almost identical to those given by (3.2.4) to (3.2.6) for the general case and to those given by (3.2.11) to (3.2.13) for the windward stagnation line case. The only difference appears in the coefficients of ff", fg" and fE'; instead of 3/2, the new equations have a coefficient of 2. It should be noted, however, that the resulting equations for turbulent flows are not strictly similar like the laminar flow equations because they were derived under the assumption of constant x. Thus, the equations are valid for a fixed x and no scaling of solutions is allowed.

3.3 Transformation of the Parabolic-Elliptic Boundary-Layer Equations

Since the PEBL equations should reproduce the 3DBL results in regions where the cross-flow gradients are not large, the same argument can be made for using a similarity transformation in these equations too. In the nondimensional PEBL variables used in Appendix A, the transformation (3.1.1) becomes

$$\xi = \int h_1 dx \qquad z = \theta \qquad \eta = \left(\frac{u_e}{\xi}\right)^{1/2} y \qquad (3.3.1)$$

where $u_e = u_e(x,\theta)$. Placing this into the PEBL equations (A.11) - (A.13) and defining a new velocity-like variable, V as

$$V = \xi \left[v \left(\frac{u_e}{\xi} \right)^{1/2} + \frac{u}{h_1} \eta_x + \frac{w}{h_2} \eta_\theta \right] \tag{3.3.2}$$

yields the following equations

x-momentum

$$uu_\xi + \frac{1}{h_2} wu_z + \frac{V}{\xi} u_\eta - K_1 uw + K_2 w^2 = \frac{1}{h_1} p_x + \frac{u_e}{\xi} u_{\eta\eta} + \frac{1}{R} \frac{1}{h_2^2} u_{zz} \tag{3.3.3}$$

-momentum

$$uw_\xi + \frac{1}{h_2} ww_z + \frac{V}{\xi} w_\eta - K_2 uw + K_1 u^2 = - \frac{1}{h_2} p_\theta + \frac{u_e}{\xi} w_{\eta\eta} + \frac{1}{R} \left(\frac{1}{h_2^2} w_{zz} \right.$$

$$\left. - 2 \frac{1}{h_2} K_2 u_z \right) \tag{3.3.4}$$

continuity

$$\left(\frac{u_e}{\xi} \right)^{1/2} \frac{\partial}{\partial \xi} \left[u \left(\frac{\xi}{u_e} \right)^{1/2} \right] - K_2 u + u_e^{1/2} \frac{1}{h_2} \frac{\partial}{\partial z} \left(w u_e^{-1/2} \right) - K_1 w + \frac{1}{\xi} V_\eta = 0 \tag{3.3.5}$$

The appearance of the u_e factor in the momentum equations (3.3.3) and (3.3.4) is somewhat unusual and could be eliminated by normalizing the velocities with their edge values. However, due to the presence of the second derivatives with respect to z now present in the equation, this would introduce more terms than are normally encountered (such as a $u_{e_{zz}}$ term) and it was deemed advisable to leave the equations as presented above. This led to a computational problem, to be discussed in Section 4.2, which was solved by a new technique also described in Section 4.2.

The boundary conditions to be imposed on this transformed set of equations are

$$\eta = 0 \qquad\qquad u = w = 0 \qquad\qquad V = 0 \tag{3.3.6a}$$

$$\eta \to \eta_\infty \qquad\qquad u \to u_e(\xi, z) \qquad\qquad w \to w_e(\xi, z) \tag{3.3.6b}$$

$$z = 0, \pi \qquad\qquad u_z = 0 \qquad\qquad w = 0 \tag{3.3.6c}$$

19

IV. NUMERICAL METHODS

4.1 Numerical Formulation of the Standard Boundary-Layer Equations

We use the Box method to solve the governing 3DBL equations. This
is a two-point finite-difference method that has successfully been applied
to two-dimensional flows by Keller and Cebeci and to three-dimensional flows by
Cebeci. A detailed description of the method is presented in [1] and [21].
For this reason only a brief description of it will be presented here.

One of the basic ideas of the Box method is to write the governing sys-
tem of equations in the form of a first-order system. Thus, in our case, the
first derivatives of f and g with respect to η are introduced as new
unknown functions. With the resulting first-order system and an arbitrary
rectangular net, we use simple centered difference quotients and averages at
the midpoints of net rectangles and net segments to get second-order accurate
finite-difference equations. Then nonlinear difference equations are linear-
ized by using Newton's method and the resulting linear system is solved by
the block-elimination method discussed by Isaacson and Keller [22].

In our present method we solve the two momentum equations simultaneously.
Essentially the stagnation-line equations and the symmetry plane equations are
two-dimensional flows in the sense that these equations have only two independ-
ent variables, (x,η) or (z,η). On the other hand, the two momentum equa-
tions (3.1.5) and (3.1.6) are three-dimensional flow equations for obvious
reasons. The solution of the two-dimensional flow equations is discussed in
considerable length in references [18], [21], for this reason we shall
only discuss the solution of three-dimensional-flow equations, namely, (3.1.5),
(3.1.6) and their boundary conditions, (3.1.19).

With the introduction of new independent variables $u(x,z,\eta)$, $v(x,z,\eta)$,
$w(x,z,\eta)$ and $t(x,z,\eta)$, the equations given by (3.1.5) and (3.1.6) can be
written as

$$f' = u \qquad (4.1.1a)$$

$$u' = v \qquad (4.1.1b)$$

$$g' = w \qquad (4.1.1c)$$

$$w' = t \qquad (4.1.1d)$$

20

$$(bv)' + m_1 fv - m_2 u^2 - m_5 uw + m_6 vg - m_8 w^2 + m_{11} = m_{10} \left(u \frac{\partial u}{\partial x} - v \frac{\partial f}{\partial x} \right)$$

$$+ m_7 \left(w \frac{\partial u}{\partial z} - v \frac{\partial g}{\partial z} \right) \quad (4.1.1e)$$

$$(bt)' + m_1 ft - m_4 uw - m_3 w^2 + m_6 gt - m_9 u^2 + m_{12} = m_{10} \left(u \frac{\partial w}{\partial x} - t \frac{\partial f}{\partial x} \right)$$

$$+ m_7 \left(w \frac{\partial w}{\partial z} - t \frac{\partial g}{\partial z} \right) \quad (4.1.1f)$$

We next consider the net cube shown in Figure 1 and introduce the net points by

$$
\begin{array}{lll}
x_0 = 0 & x_n = x_{n-1} + k_n & n = 1, 2, \ldots, N \\
z_0 = 0 & z_i = z_{i-1} + r_i & i = 1, 2, \ldots, I \qquad (4.1.2) \\
\eta_0 = 0 & \eta_j = \eta_{j-1} + h_j & j = 1, 2, \ldots, J
\end{array}
$$

The difference equations which are to approximate (4.1.1a) to (4.1.1d) are obtained by averaging about the midpoint $(x_n, z_i, \eta_{j-1/2})$
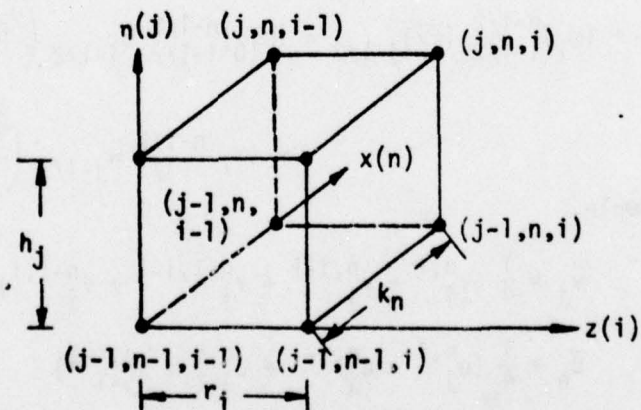
Figure 1. Net cube for the difference equations for three-dimensional flows.

21

$$\frac{f_j^{n,i} - f_{j-1}^{n,i}}{h_j} = u_{j-1/2}^{n,i} \qquad (4.1.3a)$$

$$\frac{u_j^{n,i} - u_{j-1}^{n,i}}{h_j} = v_{j-1/2}^{n,i} \qquad (4.1.3b)$$

$$\frac{g_j^{n,i} - g_{j-1}^{n,i}}{h_j} = w_{j-1/2}^{n,i} \qquad (4.1.3c)$$

$$\frac{w_j^{n,i} - w_{j-1}^{n,i}}{h_j} = t_{j-1/2}^{n,i} \qquad (4.1.3d)$$

where, for example,

$$u_{j-1/2}^{n,i} = \frac{1}{2}\,(u_j^{n,i} + u_{j-1}^{n,i})$$

The difference equations which are to approximate (4.1.1e,f) are rather lengthy. To illustrate the differencing of equations similar to (4.1.1e,f), we consider the following model equation:

$$v' + m_1 fv = m_{10} u\,\frac{\partial u}{\partial x} + m_7 w\,\frac{\partial u}{\partial z} \qquad (4.1.4)$$

The difference equations for this equation are

$$\frac{\bar{v}_j - \bar{v}_{j-1}}{h_j} + (m_1)_{i-1/2}^{n-1/2}\,(\overline{fv})_{j-1/2} = (m_{10})_{i-1/2}^{n-1/2}\,\bar{u}_{j-1/2}\left(\frac{\bar{u}_n - \bar{u}_{n-1}}{k_n}\right)$$

$$+ (m_7)_{i-1/2}^{n-1/2}\,\bar{w}_{j-1/2}\left(\frac{\bar{u}_i - \bar{u}_{i-1}}{r_i}\right) \quad (4.1.5)$$

where, for example,

$$\bar{v}_j = \frac{1}{4}\,(v_j^{n,i} + v_j^{n,i-1} + v_j^{n-1,i-1} + v_j^{n-1,i})$$

$$\bar{u}_n = \frac{1}{4}\,(u_j^{n,i} + u_j^{n,i-1} + u_{j-1}^{n,i} + u_{j-1}^{n,i-1})$$

$$\bar{u}_i = \frac{1}{4}\,(u_j^{n,i} + u_j^{n-1,i} + u_{j-1}^{n,i} + u_{j-1}^{n-1,i})$$

$$(m_1)_{i-1/2}^{n-1/2} = \frac{1}{4}\,[(m_1)_i^n + (m_1)_{i-1}^n + (m_1)_i^{n-1} + (m_1)_{i-1}^{n-1}]$$

22

The boundary conditions for the system of equations given by (4.1.1) at $x = x_n$ and at $z = z_i$ are:

$$f_0^{n,i} = 0, \quad g_0^{n,i} = 0, \quad u_0^{n-i} = 0, \quad w_0^{n,i} = 0, \quad u_J^{n,i} = 1, \quad w_j^{n,i} = \left(\frac{w_e}{u_{ref}}\right)^{n,i}$$

(4.1.6)

If we assume $(f_j^{n-1,i-1}, u_j^{n-1,i-1}, v_j^{n-1,i-1}, g_j^{n-1,i-1}, w_j^{n-1,i-1}, t_j^{n-1,i-1})$, $(f_j^{n,i-1}, u_j^{n,i-1}, v_j^{n,i-1}, g_j^{n,i-1}, w_j^{n,i-1}, t_j^{n,i-1})$, and $(f_j^{n-1,i}, u_j^{n-1,i}, v_j^{n-1,i}, g_j^{n-1,i}, w_j^{n-1,i}, t_j^{n-1,i})$ to be known for $0 \le j \le J$, then the difference equations (4.1.3) and the difference equations for (4.1.1e,f) along the (4.1.6) yield an implicit nonlinear algebraic system of $6J + 6$ equations in as many unknowns $(f_j^n, u_j^n, v_j^n, g_j^n, w_j^n, t_j^n)$. We solve this nonlinear system by means of Newton's method. The resulting linearized system is then solved by using the block elimination method discussed by Isaacson and Keller [22].

4.2 Numerical Formulation of the Parabolic-Elliptic Boundary-Layer Equations

The PEBL equation set (3.3.3) - (3.3.5) is elliptic in the cross-flow z-η plane, but still allows a parabolic march in the main flow, ξ, direction. An implicit numerical procedure was chosen to integrate these governing equations for a number of reasons. The success of implicit methods on the boundary-layer equations and parabolic-elliptic Navier-Stokes equations [23] implies that they should be efficient for the very similar PEBL equations. It is expected that solutions will be required at arbitrary points along the body; and so for convenience in the computation, to eliminate the need to check the step size restrictions of explicit methods, unconditionally stable methods (which are consistent with the original partial-differential equations of the problem) are necessary. This leads to the consideration of implicit methods.

The particular method used in this study is the alternating-direction implicit (ADI) method, used in the form originally proposed by Peaceman and Rachford [24]. The ADI method is ideally suited for the solution of (3.3.3)-(3.3.4). There is no stability restriction on the step size, and hence arbitrary ξ-steps are permitted. The method has second-order truncation error in its marching variation, which is also a requirement for the type of flow envisioned here, since the ξ-history of the flow must be traced accurately

23

at each step. Finally, the method does not require the inversion of a sparse banded matrix, as a fully implicit or Crank-Nicolson scheme would. Simple tridiagonal coefficient matrices are generated at each step which require much less storage and time for their inversion when compared with sparse matrices.

The ADI method is a two-step, second-order accurate procedure centered about the midpoint of the ξ step from $i\Delta\xi$ to $(i + 2)\Delta\xi$, i.e., at $(i+1)\Delta\xi$, for uniform Δz and $\Delta\eta$ grids. An example of its use is shown on the following equation modelling either (3.3.3) or (3.3.4).

$$N_1 u_x + N_2 u_y + N_3 u_z = N_4 + u_{zz} + u_{yy} \tag{4.2.1}$$

The two ADI steps are written

$$\frac{1}{\Delta x}(N_1)_{j,k}^{i+1}(u_{j,k}^\star - u_{j,k}^i) + (N_2)_{j,k}^{i+1}\delta_y u_{j,k}^i + (N_3)_{j,k}^{i+1}\delta_z u_{j,k}^\star$$
$$= (N_4)_{j,k}^{i+1} + \delta_z^2 u_{j,k}^\star + \delta_y^2 u_{j,k}^i \tag{4.2.2a}$$

$$\frac{1}{\Delta x}(N_1)_{j,k}^{i+1}(u_{j,k}^{i+2} - u_{j,k}^\star) + (N_2)_{j,k}^{i+1}\delta_y u_{j,k}^{i+2} + (N_3)_{j,k}^{i+1}\delta_z u_{j,k}^\star$$
$$= (N_4)_{j,k}^{i+1} + \delta_z^2 u_{j,k}^\star + \delta_y^2 u_{j,k}^{i+2} \tag{4.2.2b}$$

where the N_m, $m \leq 3$ are nonlinear coefficients, N_4 is a source term, and the standard central differencing, including the option of nonuniform spacing has been used, i.e.,

$$\delta_z u_{j,k}^i = \frac{(\Delta z_-)^2 u_{j,k+1}^i - [(\Delta z_+)^2 - (\Delta z_-)^2]u_{j,k}^i - (\Delta z_+)^2 u_{j,k-1}^i}{(\Delta z_+)(\Delta z_-)[(\Delta z_+) + (\Delta z_-)]} \tag{4.2.3a}$$

$$\delta_z^2 u_{j,k}^i = 2\left\{\frac{(\Delta z_-)u_{j,k+1}^i - [(\Delta z_+) + (\Delta z_-)]u_{j,k}^i + (\Delta z_+)u_{j,k-1}^i}{(\Delta z_+)(\Delta z_-)[(\Delta z_+) + (\Delta z_-)]}\right\} \tag{4.2.3b}$$

The pressure gradient portion of N_4, since it is a known, prescribed function, given by the external flow at all the marching steps, is computed from

$$p_x)^{i+1} = \frac{1}{2}[p_x)^i + p_x)^{i+2}] \tag{4.2.4}$$

24

and not simply evaluated at the (*) station, which is only a temporary
integration location, and does not correspond to the physical midpoint $(i + 1)$.
The remaining N_m are given by a second-order extrapolation (of consistent
accuracy with the integration procedure) from previously computed x-stations.
Originally, the standard extrapolations were used. These are derivable from
Taylor's series, i.e.,

$$Q^{i+1} = \left(1 + \frac{\Delta x_+}{2\Delta x_-}\right) Q^i - \frac{\Delta x_+}{2\Delta x_-} Q^{i-2} \qquad (4.2.5a)$$

or

$$Q^{i+1} = \left(1 + \frac{\Delta x_+ + \Delta x_-}{\Delta x_- + \Delta x_=}\right) Q^{i-1} - \left(\frac{\Delta x_+ + \Delta x_-}{\Delta x_- + \Delta x_=}\right) Q^{i-3} \qquad (4.2.5b)$$

depending upon where the variables are stored. However, since the values of
the dependent variables used in the PEBL equations, (3.3.3)-(3.3.5) were not
normalized by their edge values, this procedure yields spurious results near
the edge of the boundary layer and in the inviscid portion of the flow. A
simple correction for this difficulty has been found [25], and incorporated
into the PEBL-ADI integration procedure. It consists of incorporating the
known information about the edge velocities into the linearization so that it
correctly predicts the midpoint values at $(i + 1)$. This is accomplished by

$$Q_c^{i+1} = C \, Q^{i+1} \; ; \quad C = \frac{[(Q_e^i + Q_e^{i+2})/2]}{[(1 + \Delta x_+/2\Delta x_-)Q_e^i - (\Delta x_+/2\Delta x_-)Q_e^{i-2}]} \qquad (4.2.6)$$

where the Q^{i+1} in (4.2.6) is the usual value given in (4.2.5a).

In this way, the two momentum equations are decoupled from each other
and the continuity equation (3.3.5), and the integration can proceed without
iteration. After the complete two-step ADI procedure is completed, the solu-
tion obtained is second-order accurate, centered at $(i + 1)\Delta\xi$. It is at this
ξ-station that the continuity equation is evaluated. The unknown velocity
$\bar{V}(\xi,z,\eta)$ can be computed at the given ξ-station successively out from the wall,
where the boundary condition $\bar{V}(\xi,z,0) = 0$ holds, to the edge of the computa-
tional domain, and around the cone from the windward to leeward meridian.
This is accomplished by differencing equation (3.3.5) as follows

25

$$\overline{\delta}_\eta V_{j-1/2,k}^{i+1} = -\frac{1}{2} u_{j-1/2,k}^{i+1} - \xi^{i+1}\left[\overline{\delta}_\xi u_{j-1/2,k}^{i+1} - \left(K_2 + \frac{1}{2}\frac{u_{e_\xi}^{i+1}}{u_e^{i+1}}\right)u_{j-1/2,k}^{i+1}\right.$$

$$\left. + \frac{1}{h_2}\delta_z w_{j-1/2,k}^{i+1} - \left(K_1 + \frac{1}{h_2}\frac{u_{e_z}^{i+1}}{u_e^{i+1}}\right)w_{j-1/2,k}^{i+1}\right] \qquad (4.2.7)$$

where

$$\overline{\delta}_\eta V_{j-1/2,k}^{i+1} = \frac{V_{j,k}^{i+1} - V_{j-1,k}^{i+1}}{\Delta n_j} \qquad ; \qquad \overline{\delta}_\xi u_{j-1/2,k}^{i+1} = \frac{u_{j-1/2,k}^{i+2} - u_{j-1/2,k}^{i}}{2\Delta\xi}$$

δ_z is defined by (4.2.3a) and all the indicated differentiations in (3.3.5) have been performed.

The differencing (4.2.2) generates tridiagonal matrices for each unknown at both values of the ADI step, which are easily solved by the familiar algorithm. The only alteration from the straightforward application of the integration takes place on the z-implicit step for the u-velocity. Here, the boundary conditions to be applied are zero gradient at both boundaries, see (3.3.6c). Rather than differencing the equation on the boundaries and using fictitious nodes to fulfill boundary conditions, the integration domain was limited to include all but the boundary points. The boundary condition was then incorporated by using a second-order accurate one-sided difference to define the values of the first and last points in terms of its nearest neighbors as follows:

$$u_{1,k} = \frac{(\Delta z_2 + \Delta z_3)^2 u_{2,k} - \Delta z_2^2 u_{3,k}}{[(\Delta z_2 + \Delta z_3)^2 - \Delta z_2^2]}$$

$$(4.2.8)$$

$$u_{JMAX,k} = \frac{(\Delta z_{JMAX} + \Delta z_{JMAX-1})^2 u_{JMAX-1,k} - \Delta z_{JMAX}^2 u_{JMAX-2,k}}{[(\Delta z_{JMAX} + \Delta z_{JMAX-1})^2 - \Delta z_{JMAX}^2]}$$

The procedure does not destroy the tridiagonal nature of the coefficient matrix, and has been used with success previously [23].

26

V. RESULTS

5.1 Body of Revolution

The test case chosen as a standard for all the body of revolution comparisions to be given below is the flow past a prolate spheroid, as shown in figure 2, whose axis ratio, t, equals 1/4.

The solution to the three-dimensional boundary-layer equations, written in a general orthogonal body-oriented coordinate system requires the prescription of the body geometry, and derivable from that, the external potential flow. In order to assess the accuracy of the boundary-layer solution, an analytically-prescribed body with reasonably simple closed form solutions for the potential flow was used. This avoids the problems caused by trying to spline fit and smooth numerically computed surfaces and velocity components. It must be emphasized that this simple body is not necessary for the successful use of the computer program, and general geometry packages are available [1]. Thus, the calculations were performed over a simple body of revolution, namely, the prolate spheroid. This configuration was previously considered by Wang [12] - [14] who has documented the resulting flow field at various angles of attack. This body has extensive regions of cross-flow reversal within a still unseparated region and, in addition, has an unusual separation pattern at moderate angles of attack which makes it an excellent test case on which to perform three-dimensional boundary-layer studies. It is felt that the extension to compressible flow will not be more than a minor alteration to the procedures developed here. Similarly, the inclusion of turbulence can be easily accomplished for three-dimensional boundary layers by the means of the eddy-viscosity model described in Section 2.4, and used in the following section for conical flows. What is essential is the verification of the methods to be used for such computations. Hence this study dealt with incompressible flow in order to determine the features of the two numerical techniques proposed.

For the prolate spheroid depicted in figure 2 we can write the equation of the surface

$$x^2 + \frac{r^2}{t^2} = 1 \tag{5.1.1}$$

27
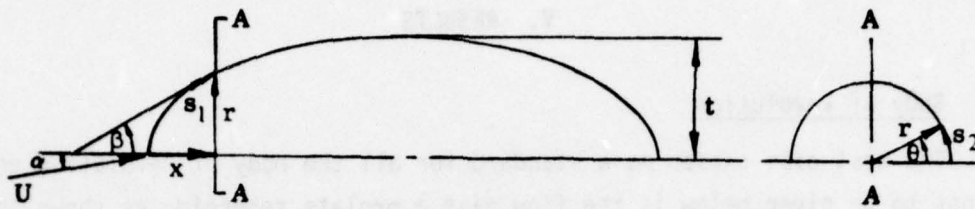
Figure 2. Geometry of the prolate spheroid.

and the incremental distance along the surface

$$ds_1^2 = dr^2 + dx^2$$

Thus

$$\left(\frac{ds_1}{dx}\right)^2 = 1 + \left(\frac{dr}{dx}\right)^2$$

and using eq. (5.1.1) gives

$$\left(\frac{ds_1}{dx}\right)^2 = \frac{1 + x^2(t^2 - 1)}{(1 - x^2)}$$

But, from figure 2, we have

$$\cos\beta = \frac{dx}{ds_1} \qquad (5.1.2)$$

Hence

$$\cos\beta = \left[\frac{(1 - x^2)}{1 + x^2(t^2 - 1)}\right]^{1/2} \qquad \sin\beta = \frac{-xt}{[1 + x^2(t^2 - 1)]^{1/2}} \quad (5.1.3)$$

The metric coefficients are determined from

$$ds_1 = h_1 dx \qquad\qquad ds_2 = h_2 d\theta$$

thus, from figure 2 and eq. (5.1.1),

$$ds_2 = rd\theta = t(1 - x^2)^{1/2} d\theta$$

and from eq. (5.1.2)

$$ds_1 = \frac{1}{\cos\beta} dx$$

28

Consequently,

$$h_1 = \left[\frac{1 + x^2(t^2 - 1)}{(1 - x^2)}\right]^{1/2} \qquad\qquad h_2 = t(1 - x^2)^{1/2} \qquad (5.1.4)$$

and the curvatures are

$$K_2 = \frac{x}{[1 + x^2(t^2 - 1)]^{1/2}(1 - x^2)^{1/2}} , \qquad K_1 = 0 \qquad (5.1.5)$$

These geometrical relationships are used in the governing equations of boundary-layer flow and also in the determination of the potential. From Faulkner et al. [26], the velocity components on the surface of a prolate spheroid are given by

$$\frac{V_{s_1}}{V_\infty} = V_0(t)\cos\alpha\,\cos\beta - V_{90}(t)\sin\alpha\,\sin\beta\,\cos\theta \qquad (5.1.6)$$

$$\frac{V_\theta}{V_\infty} = V_{90}(t)\sin\alpha\,\sin\theta \qquad (5.1.7)$$

where the various angles α, β and θ are depicted in figure 2, and the functions V_0 and V_{90} are only functions of t, the thickness of the body, given by [26]

$$V_0(t) = \frac{(1 - t^2)^{3/2}}{\sqrt{1 - t^2} - 1/2\, t^2\,\ln\left[(1 + \sqrt{1 - t^2})/(1 - \sqrt{1 - t^2})\right]} \qquad (5.1.3)$$

$$V_{90}(t) = \frac{2V_0(t)}{2V_0(t) - 1} \qquad (5.1.9)$$

Equations (5.1.4) - (5.1.9) are all the input necessary to the boundary-layer equations for the flow past a prolate spheroid.

The initial calculation made was simply the prolate spheroid at zero degrees incidence, i.e., axisymmetric flow. While this is a trivial case for the standard 3DBL procedure (it calculates one attachment-line flow, and the result is valid at every angular position around the body), it has to be

demonstrated that the PEBL procedure, which by its very nature <u>must</u> calculate all the points around the body, generates axisymmetric flow. Consequently, the PEBL procedure was used for the axisymmetric case using only five points around the body, i.e., $\Lambda\theta = 0.78539$ (45°), a very crude grid. The grid spacings across the boundary layer and down the body were identical to those used previously for 3DBL, i.e., $\Delta\eta = 0.3$ and Δx varying up to 0.1 for $x > -0.5$. As in all cases to be discussed, the initial data planes necessary for the extrapolation in (4.2.5) were obtained from the standard boundary-layer calculation.

The results of this calculation showed that the initially axisymmetric boundary layer remained that way until the separation point was reached. The computed values of w, which are exactly zero for axisymmetric flow, were all of the order of 10^{-8} (below the round-off error of the single precision arithmetic of the IBM machine used). The differences in the u velocity around the body occurred in the fifth decimal place, again close to round-off error.

The plot shown in figure 3, gives a comparison of f_w'', the wall shear parameter, obtained by both methods. The curves are effectively indistinguishable until the effects of the adverse pressure gradient at the rear of the body are felt. Here, one would expect the lack of iteration in the PEBL procedure to generate less accurate results than the 3DBL procedure which uses a Newton iteration. Nevertheless, the results are fairly good, and the axisymmetry is indeed maintained by the PEBL procedure only by the imposition of symmetry conditions, c.f. (3.2.6c), at the windward and leeward meridians.

The 3DBL results were next compared with the published results of Wang for the axisymmetric case [12]. The skin friction (in Wang's notation) down the body computed by both methods is shown in figure 4. There is a noticeable difference between the two calculations with separation predicted at $x \simeq 0.675$ and $x \simeq 0.8$ by the 3DBL or PEBL calculation and Wang, respectively. An independent calculation of this same problem made by Chang [27], substantiates our results.

The next test case considered was chosen to generate just a small amount of crossflow. The incidence of the flow was taken to be 2°. The general
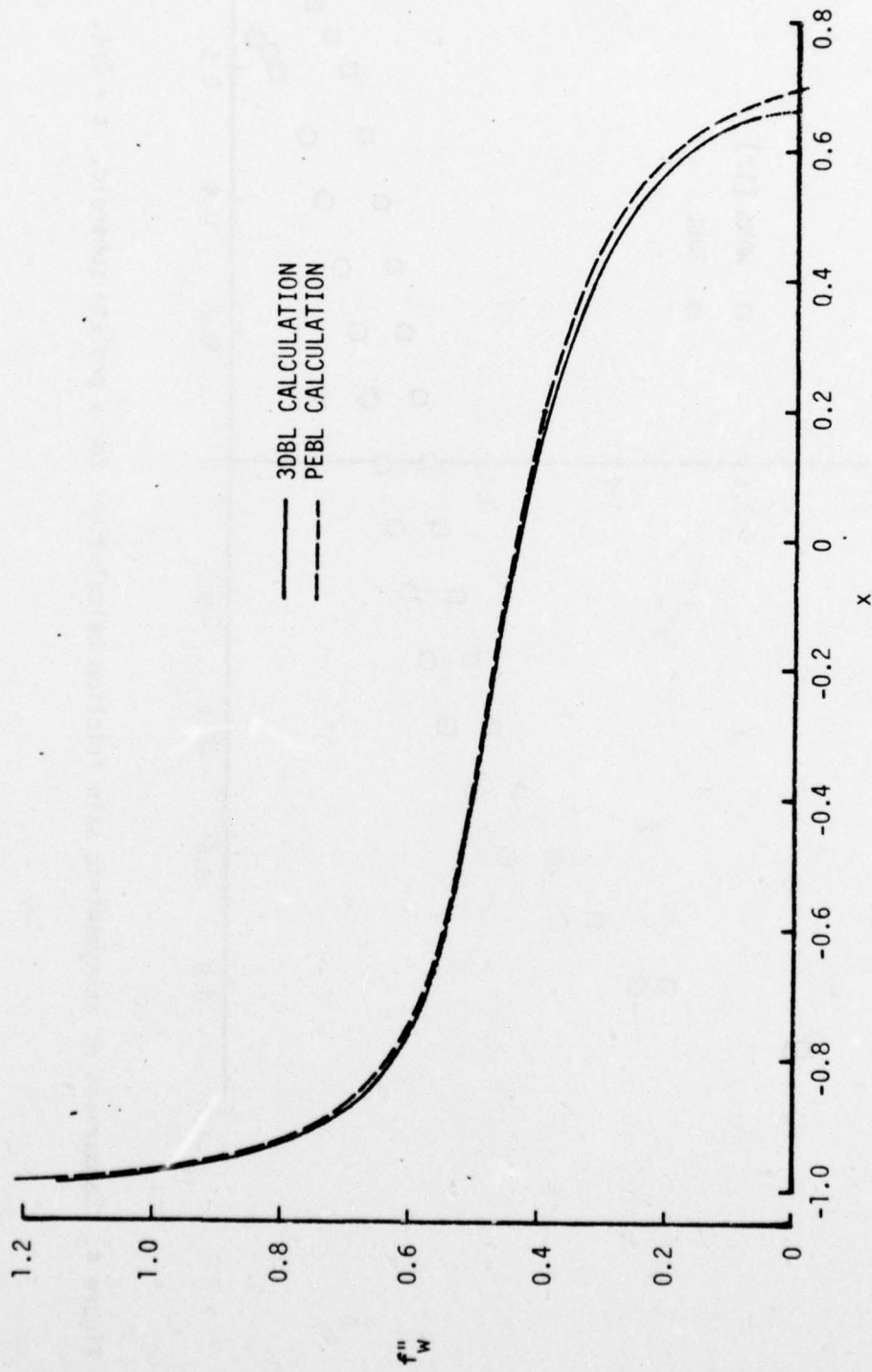
Figure 3. Comparison of skin-friction calculations for a prolate spheroid, t = 1/4, at 0° incidence.
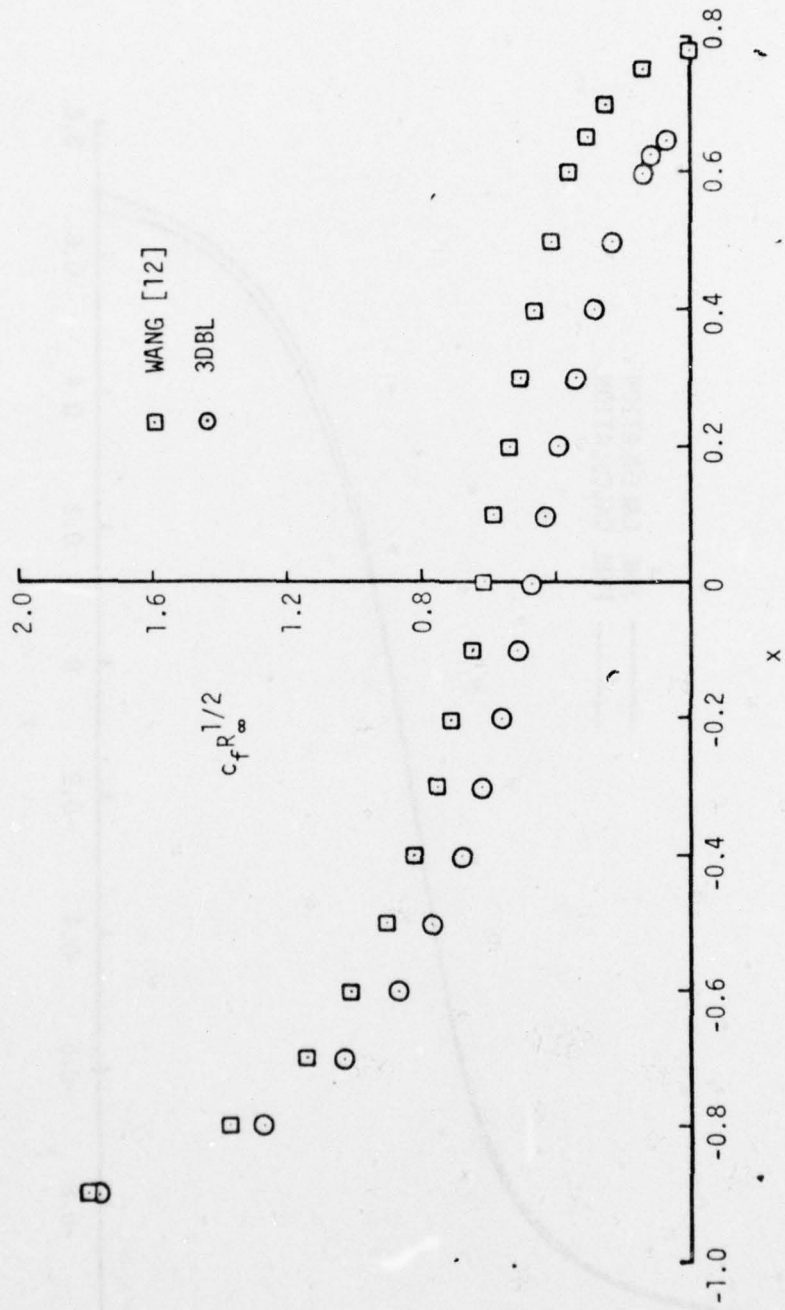
Figure 4. Comparison of axisymmetric skin friction calculations for a prolate spheroid, t = 1/4.

structure of the flow near the body is shown in fig. 5. The ordinate repre-
sents the azimuthal position around the body, and the abscissa is the x
coordinate measured along the major axis. The body surface is thus the plane
of the figure. Results from two separate calculations, in addition to some
points extrapolated from Wang's study [12] are shown on this figure. The
triangles represent calculations made using the 3DBL method. To the left of
the triangles, both components of the shear stress, $\tau_x \sim \partial u / \partial y$ and
$\tau_z \sim \partial w / \partial y$, are positive. The open triangles represent the grid points at
which the crossflow shear, τ_z, reverses sign, as calculated by 3DBL. Hence
the region covered by the triangles represents a region of reverse crossflow
in the boundary-layer flow past the prolate spheroid. Computed separation
takes place at the points given by the solid triangles. Beyond 130° the grid
was too coarse in x to detect any separation for $x > 0.4$. Note that the
locus of separation points in some sense parallels the line of reverse cross-
flow.

This configuration was next calculated using the PEBL procedure. Again
on Fig. 5, the open circles represent the first locations at each x-station
where $\tau_z < 0$. The locus of these points has been approximated by the curved
line. It is obvious that it coincides with the prediction of the 3DBL calcu-
lation for the onset of reverse crossflow. There is, however, a large
discrepancy in the predicted separation point. The PEBL procedure first
senses separation along the $x = 0.65$ line almost on the entire lee surface,
$130° \leq \theta \leq 180°$, see straight line on Fig. 5. This includes a region which
was not accessible to the 3DBL calculation due to its predicted separation.
It should be noted that the region $x > 0.65$ computed by the 3DBL method for
$\theta \leq 40°$ was not accessible to PEBL. The discussion of the inability of the
3DBL to compute the entire lee-side region will be postponed until the higher
angle of attack case is considered. The region computed by 3DBL which was not
computed by PEBL is not calculable by the standard PEBL procedure set forth
here. Since all the θ stations are coupled together during the calculation,
when one station encounters separation and cannot advance into the reverse
flow, it automatically precludes the further advance of all the other stations,
i.e., only the most upstream separation point will be predicted. Thus, as
will be seen again later, one point of $\tau_x < 0$ stops the calculation. This

33
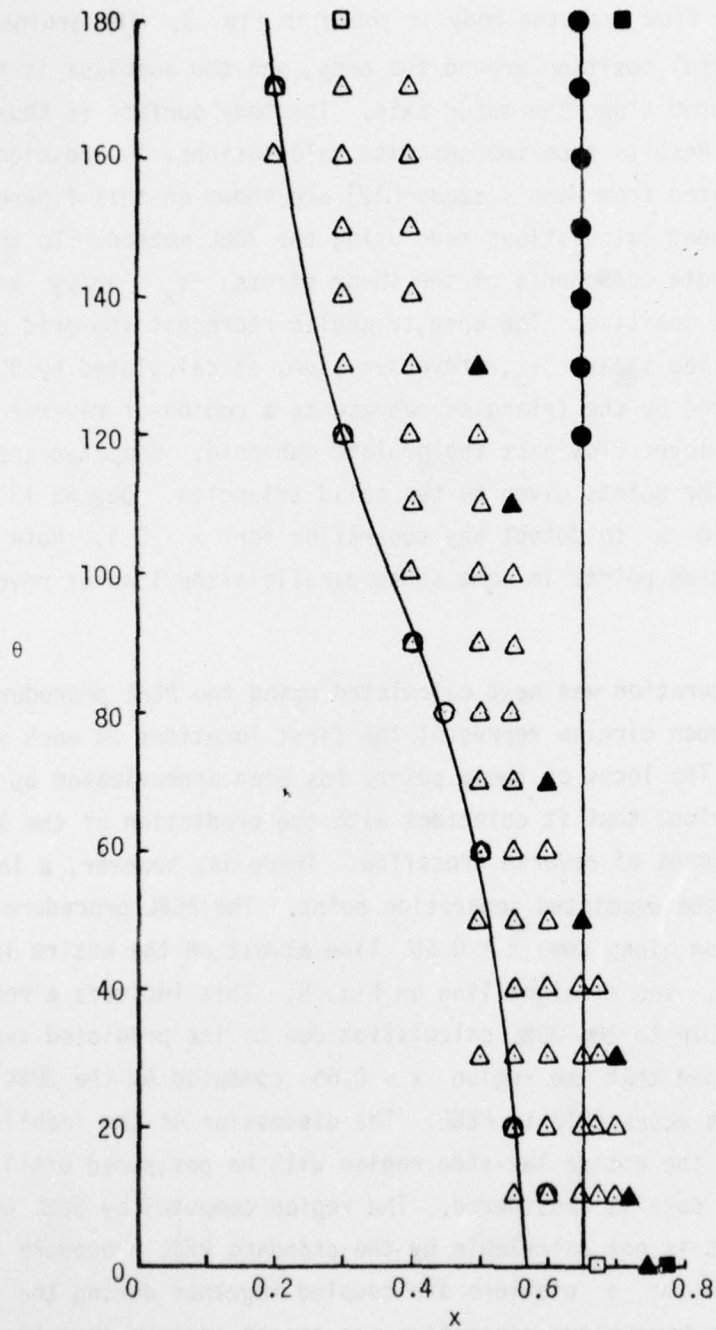
Figure 5. Calculated surface shear distributions for prolate spheroid at 2°
incidence; see text for symbol key.

is not the case for the 3DBL where, as long as the separation line sweeps upstream in x in the direction of the θ integration, the calculation can continue.

To test the PEBL calculations on their behavior approaching separation, Fig. 6 shows a plot of τ_x^2 against x. This should give a linear curve approaching separation. Stations at 160° and 170° are shown as the most relevant since there the u velocity flow will most nearly be perpendicular to the predicted separation line. The figure shows that, at least at these two stations, the calculation reproduces a square-root singularity at separation. A further check on the calculations can be made by using values of the shear on the two symmetry planes for $\alpha = 2°$ interpolated from Wang's calculations. The open squares in Fig. 5 show the location of crossflow reversal and the solid squares indicate separation. At $\theta = 0°$, the 3DBL agrees with Wang's results, and at $\theta = 180°$, the PEBL agreement is also good despite the lack of iteration.

Comparisons of the streamwise variation of the two components of shear for both 3DBL and PEBL calculations are given in Figs. 7 and 8. It is difficult to make any clear judgements between the methods. When the crossflow is unidirectional, there is little variation in f'' until crossflow reversal occurs. There the variation, and even the trend in some cases, increases. For the more sensitive crossflow g'' as the adverse pressure gradient increases for $x > 0$, the disagreement increases.

One further point can be made. The separation and crossflow reversal patterns computed for this low angle of attack case, $\alpha = 2°$, fit within the originally conceived structure set forth by Wang in his early paper [12].

When the angle of attack is increased from 2° to 6°, new features of the flow emerge, and a clearer understanding of the reasons for some of the behavior computed for the $\alpha = 2°$ case can be obtained. The first general result to consider is again the distribution of the surface shear over the entire body; see Fig. 9. As for the 2° case, this figure is a composite of two separate calculations, PEBL and 3DBL, and also includes data from Wang who gave a detailed map of the shear for this 6° incidence case [14]. The line of crossflow reversal, as computed by Wang, connects the open squares;

35
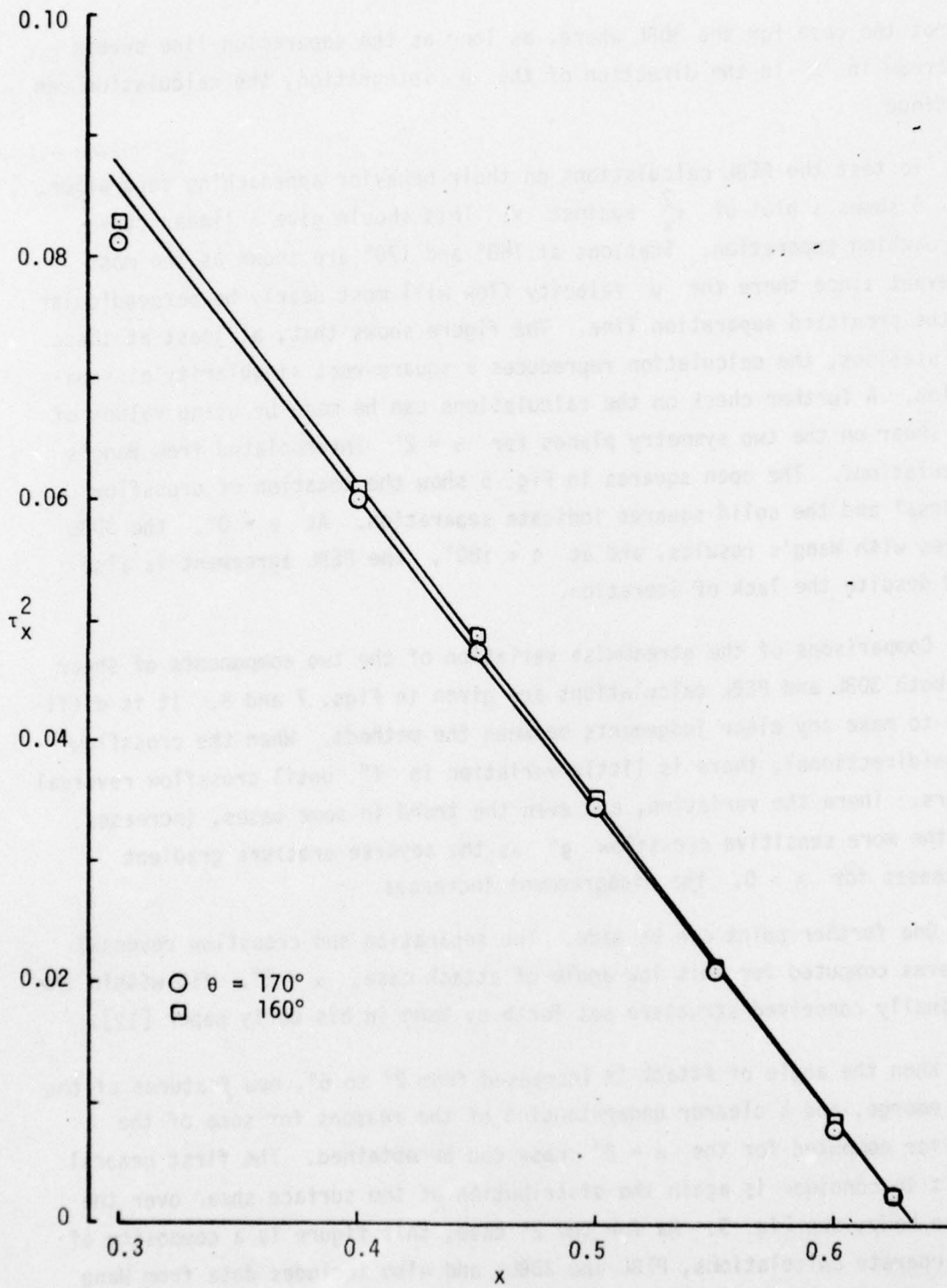
Figure 6. Approach to separation of PEBL procedure for 2° incidence case.
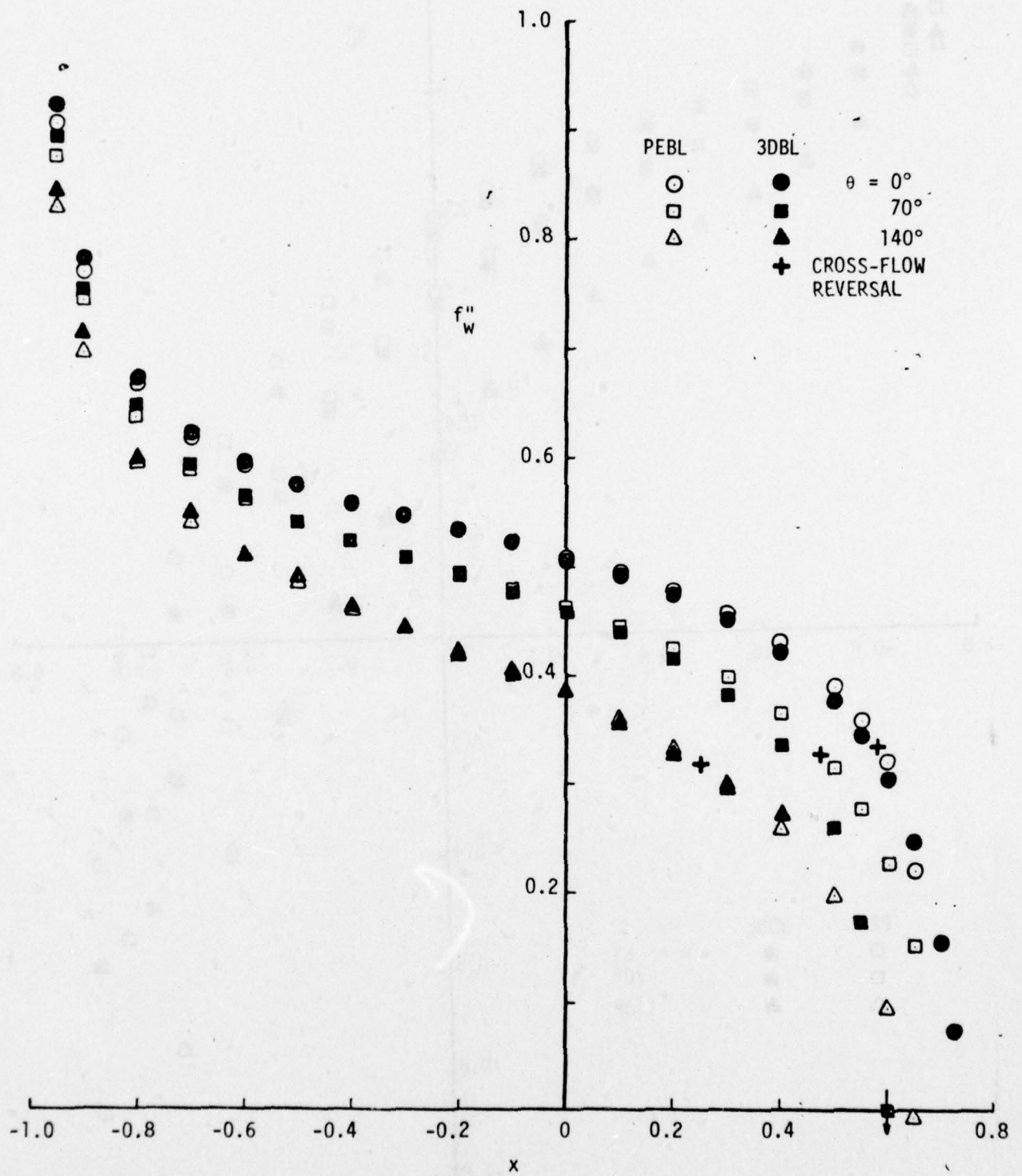
Figure 7. Streamwise surface shear variation on prolate spheroid at 2° incidence for three azimuthal locations.
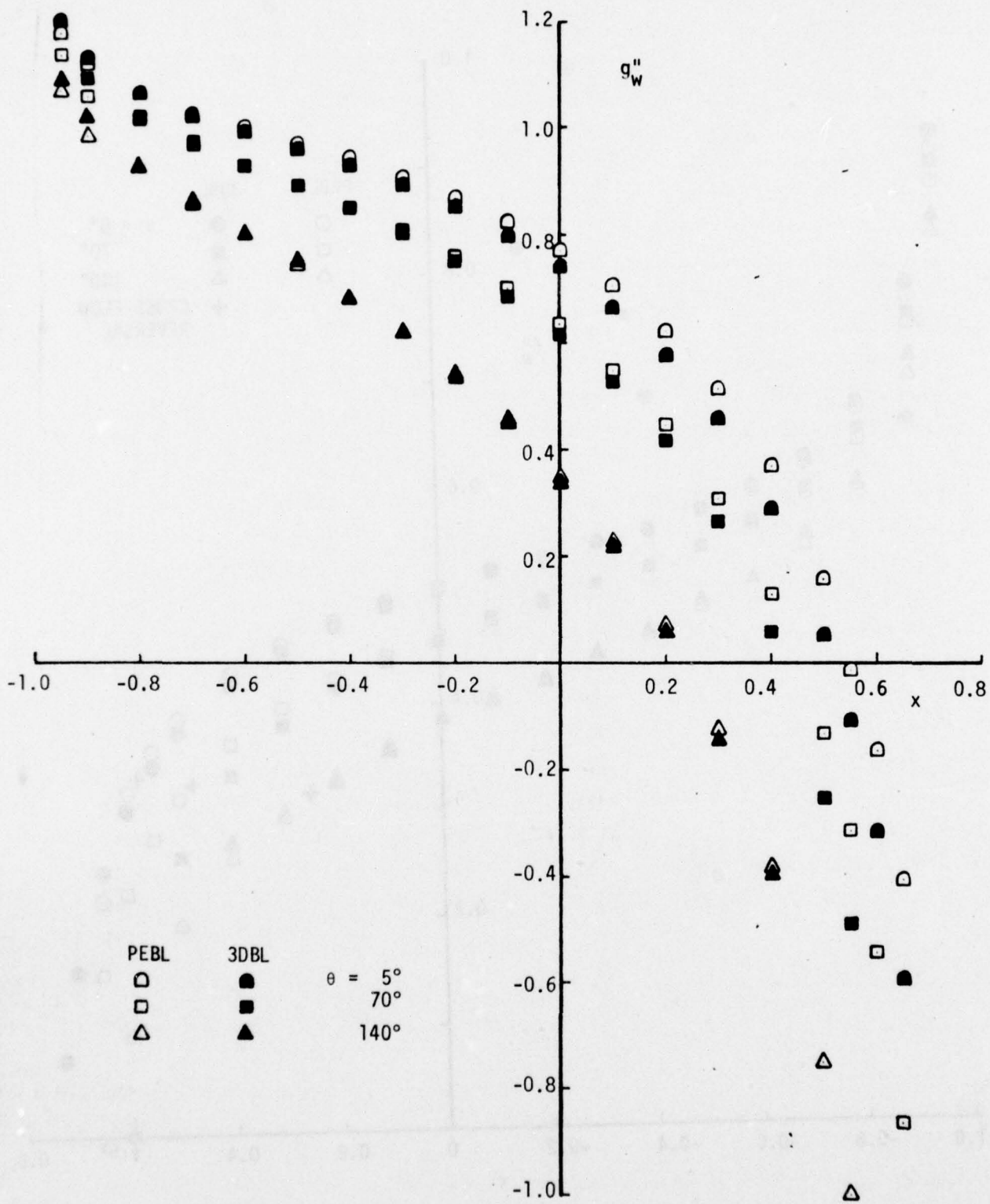
Figure 8. Cross-stream surface shear variation on prolate spheroid at 2° incidence for three azimuthal locations
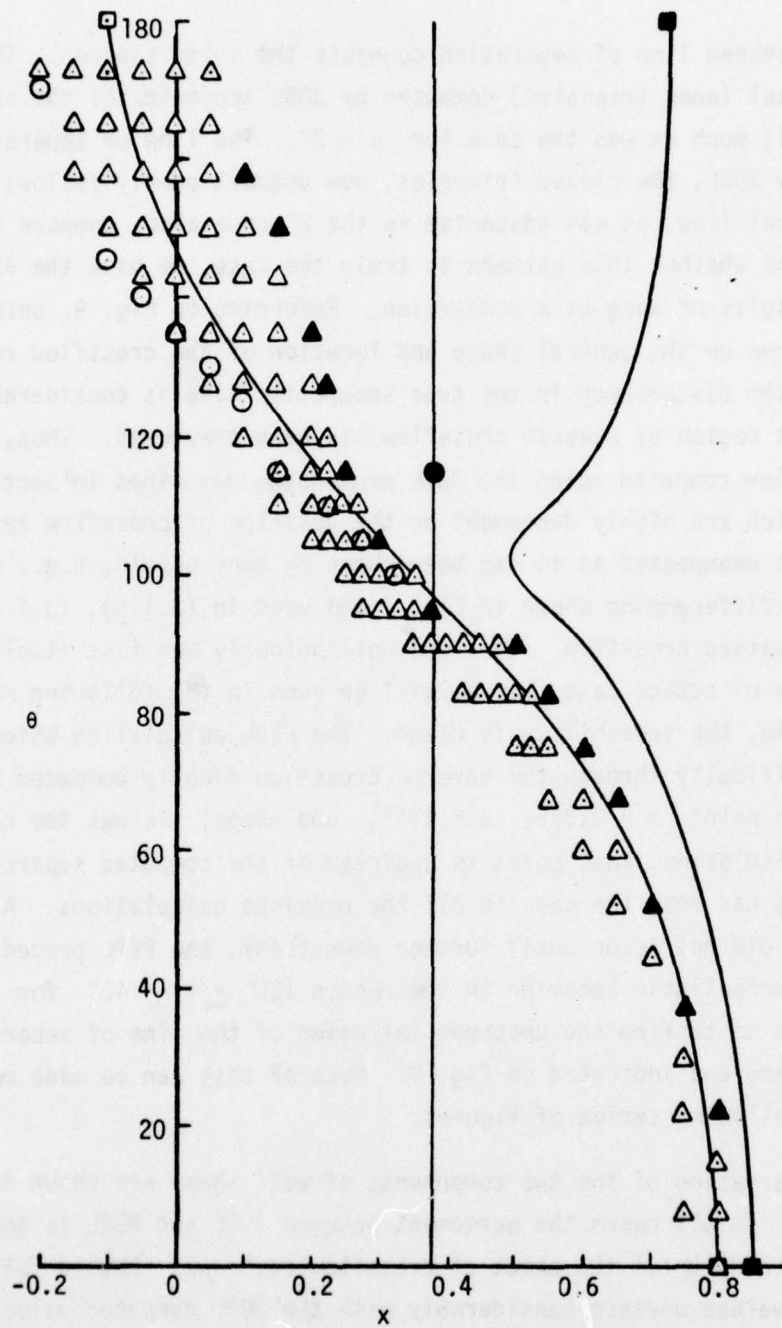
Figure 9. Calculated surface shear distributions for prolate spheroid at 6°
incidence; see text for symbol key.

the oddly shaped line of separation connects the solid squares. The cross-
flow reversal (open triangles) computed by 3DBL approximates the solid line
fairly well; much as was the case for $\alpha = 2°$. The line of separation as
computed by 3DBL, the closed triangles, now unquestionably follows the cross-
flow reversal line, as was suspected in the 2° case also, compare Fig. 5.
To determine whether this pattern is truly the case, we have the PEBL results
and the results of Wang as a comparison. Referring to Fig. 9, both other
methods agree on the general shape and location of the crossflow reversal
line, but the discrepancy in the true separation line is considerable once a
significant region of reverse crossflow has been traversed. Thus, it appears
that the flow computed using the 3DBL procedures described in Section 4.1 gives
results which are highly dependent on the position of crossflow reversal.
This is not unexpected as it has been shown by many people, e.g., Krause [28],
that the z-differencing shown in Fig. 1 and used in (3.1.5), (3.1.6) is unstable
for any negative crossflow. This did not obviously manifest itself in the
lower angle of attack case, but as will be seen in the following results to
be presented, the instability is clear. The PEBL calculation which proceeds
without difficulty through the reverse crossflow finally computed separated
flow at one point $x = 0.375$, $\theta = 115°$, and stops. As was the case for the
$\alpha = 2°$ calculation, this point is upstream of the computed separation line
of Wang, as has been the case in all the previous calculations. Although
separation did not occur until further downstream, the PEBL procedure did
calculate unrealistic behavior in the region $120° \le \theta \le 140°$ for $x > 3.0$
which tends to confirm the upstream intrusion of the line of separation com-
puted by Wang and indicated on Fig. 9. Much of this can be made more clear
from the following series of figures.

The variation of the two components of wall shear are shown in figures
10 and 11. In all cases the agreement between 3DBL and PEBL is good along
the entire body until the onset of crossflow reversal. Beyond this point,
the shear values deviate considerably with the 3DBL computed values showing
an abrupt break in the previous smooth trend. The PEBL calculations continue
with no difficulty until the adverse pressure gradient makes the extrapola-
tion process somewhat questionable. Close to separation, the computed values
of f'' between $120° \le \theta \le 140°$ show a minimum and then begin to rise. This
can be seen in the $\theta = 135°$ plot in Fig. 10 and in Fig. 12. This behavior
is certainly unrealistic and indicates a breakdown of the PEBL computation

40
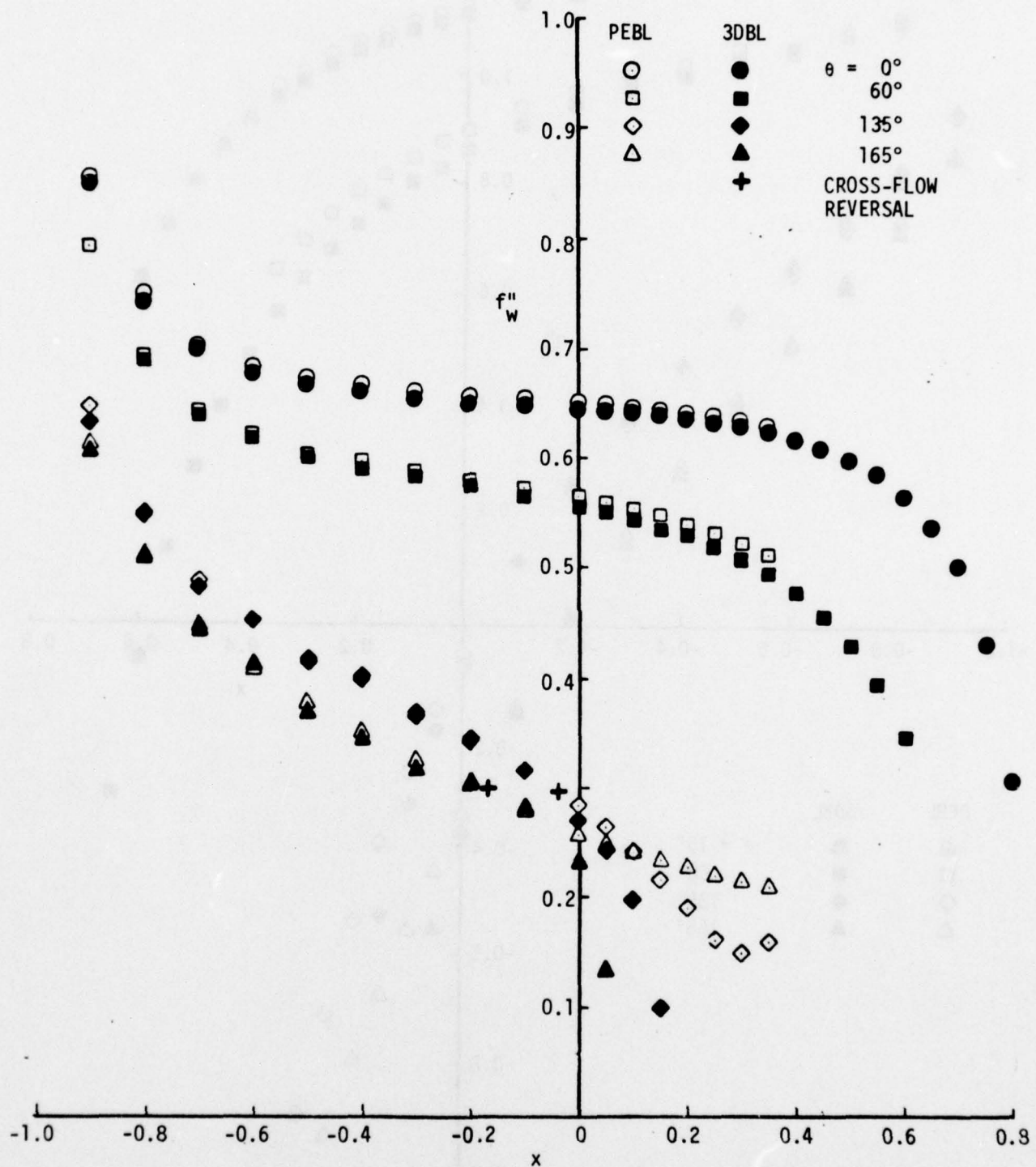
Figure 10. Streamwise surface shear variation on prolate spheroid at 6° incidence for four azimuthal locations.

41
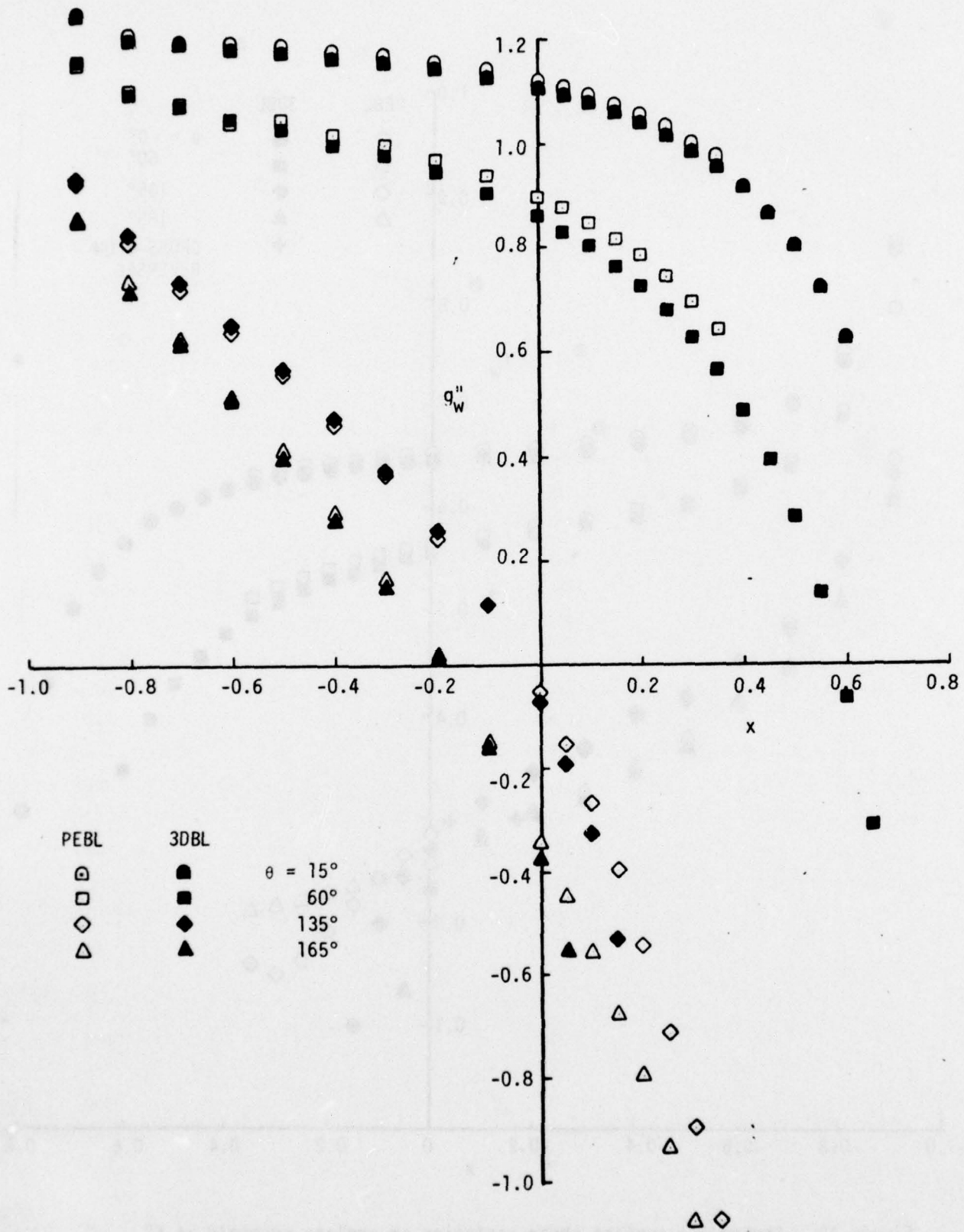
Figure 11. Cross-stream surface shear variation on prolate spheroid at 6°
incidence for four azimuthal locations.
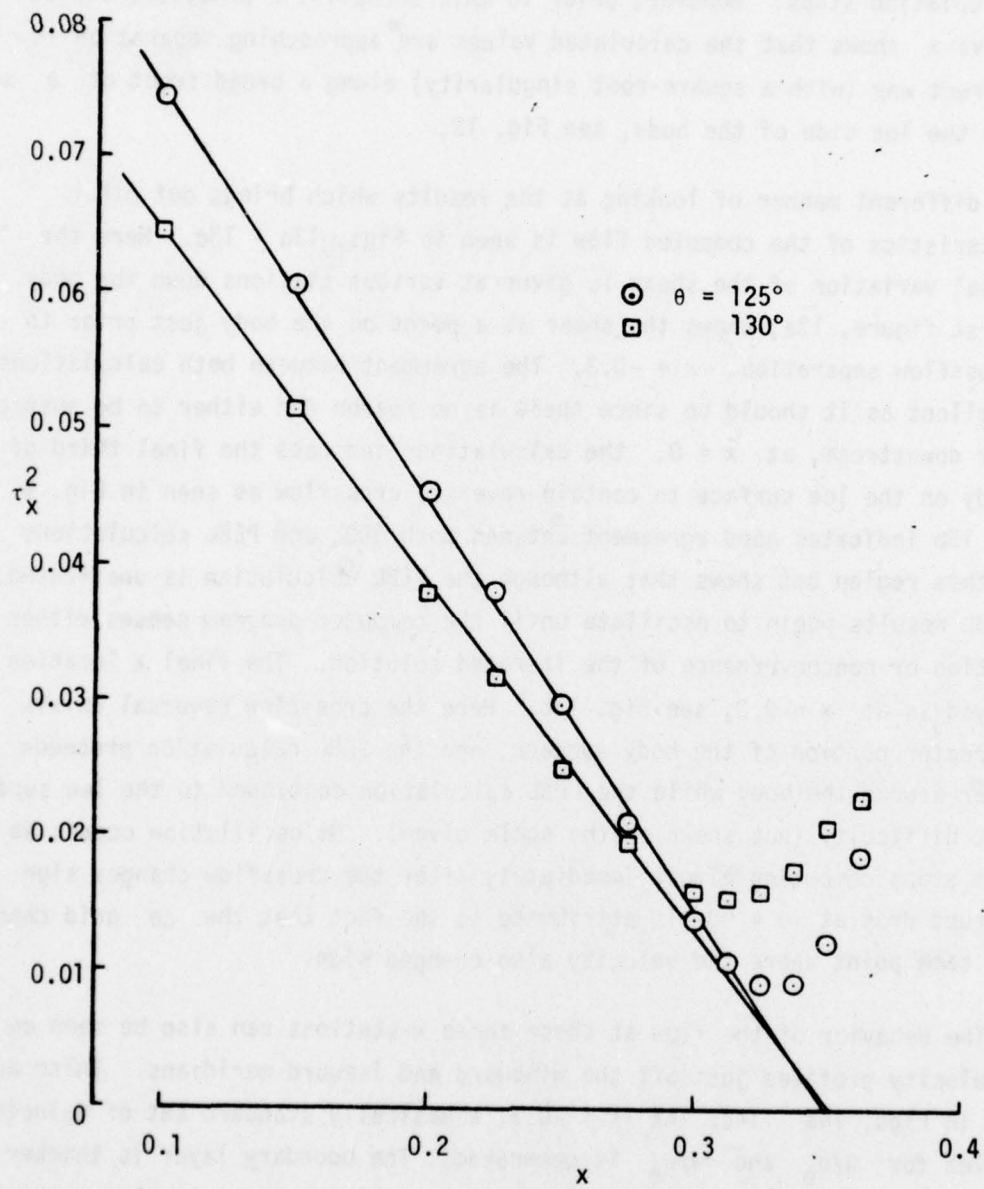
Figure 12. Approach to separation of PEBL procedure for 6° incidence case.

in the odd interior region of the flow where Wang predicts separation. A negative u velocity is sensed by the program at $\theta = 115°$, $x = 0.375$, and the calculation stops. However, prior to this unrealistic behavior, a plot of τ_x^2 vs x shows that the calculated values are approaching separation in the correct way (with a square-root singularity) along a broad front of θ just on the lee side of the body, see Fig. 12.

A different manner of looking at the results which brings out other characteristics of the computed flow is seen in Figs. 13a - 13c. Here the azimuthal variation of the shear is given at various stations down the body. The first figure, 13a, shows the shear at a point on the body just prior to any crossflow separation, $x = -0.3$. The agreement between both calculations is excellent as it should be since there is no reason for either to be suspect. Further downstream, at $x = 0$, the calculations indicate the final third of the body on the lee surface to contain reversed crossflow as seen in Fig. 9. Figure 13b indicates good agreement between both 3DBL and PEBL calculations until this region but shows that although the PEBL calculation is unaffected, the 3DBL results begin to oscillate until the computer program senses either separation or nonconvergence of the iterated solution. The final x location displayed is at $x = 0.3$, see Fig. 13c. Here the crossflow reversal exists on a greater portion of the body surface, and the 3DBL calculation proceeds less far around the body while the PEBL calculation continued to the lee surface without difficulty (not shown on the scale given). No oscillation occurs as the program stops computing almost immediately after the crossflow changes sign. The abrupt drop at $\theta = 90$ is attributed to the fact that the $\Delta\theta$ grid changed at the same point where the velocity also changed sign.

The behavior of the flow at these three x-stations can also be seen on the velocity profiles just off the windward and leeward meridians. These are shown in Figs. 14a - 14c. At $x = -0.3$, a basically standard set of velocity profiles for u/u_e and w/w_e is generated. The boundary layer is thicker near the lee side, and no unusual behavior is noticed except in the w profile at 175°, which has a slight inflection due to the adverse azimuthal pressure gradient. By $x = 0$ the crossflow on the lee side contains a small layer of reversed flow. The streamwise flow on the lee side has become less full, and the thickness of the boundary layer here has increased. On the windward side, the shape and thickness of both u and w profiles have

44
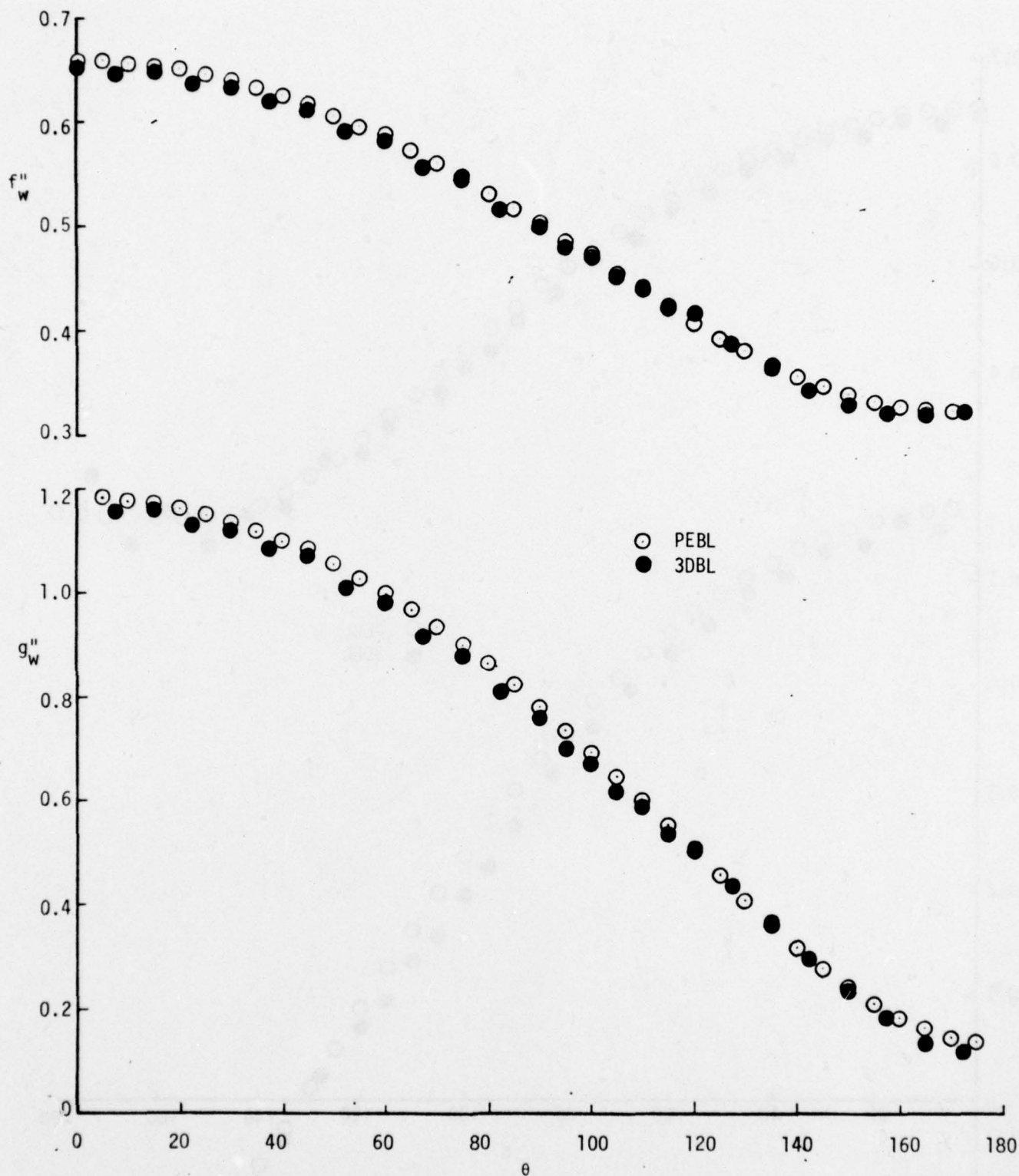
Figure 13. Azimuthal variation of streamwise and cross-stream surface shear for 6° incidence; (a) x = -0.3.

45
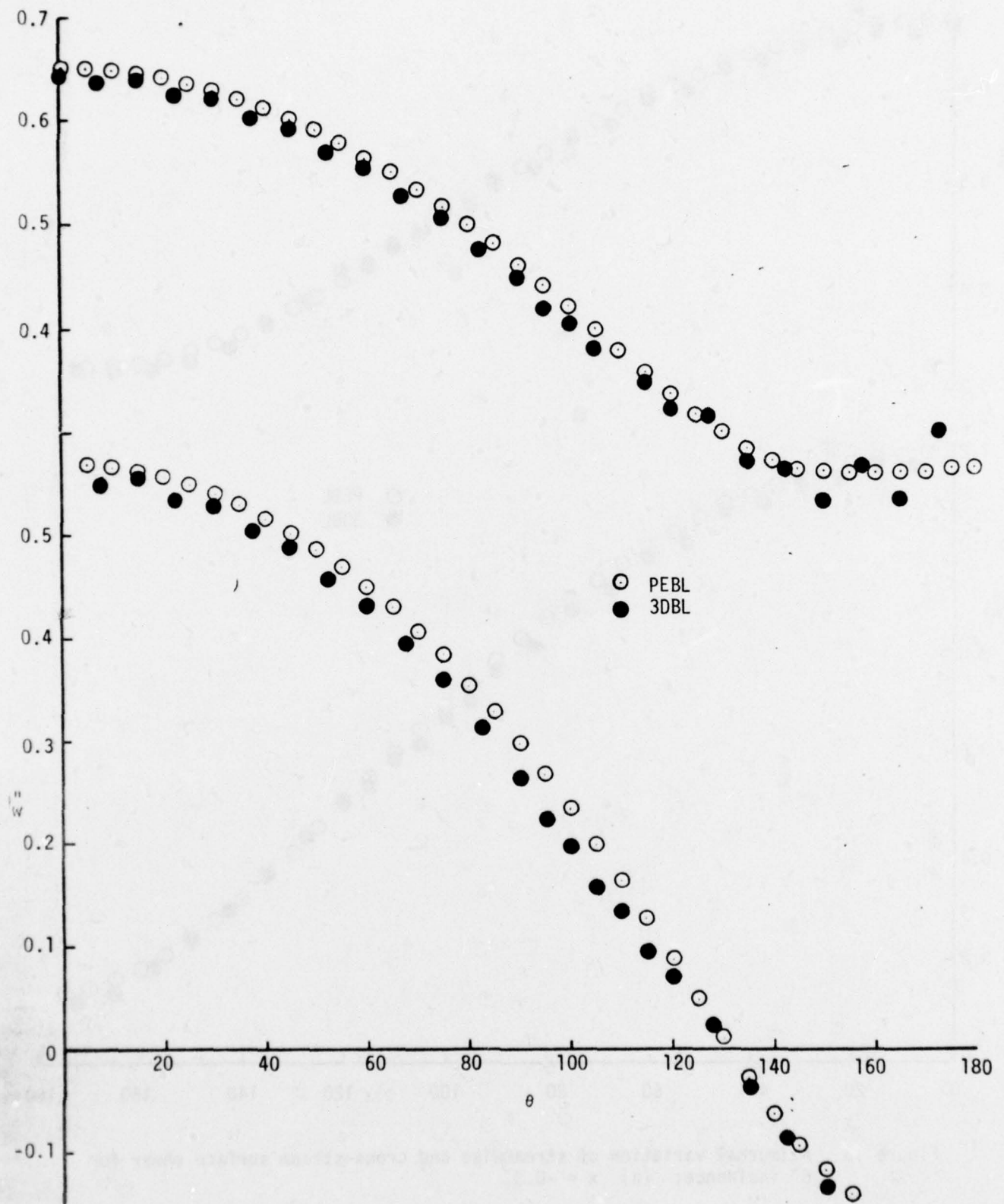
Figure 13. Continued (b) x = 0.

46
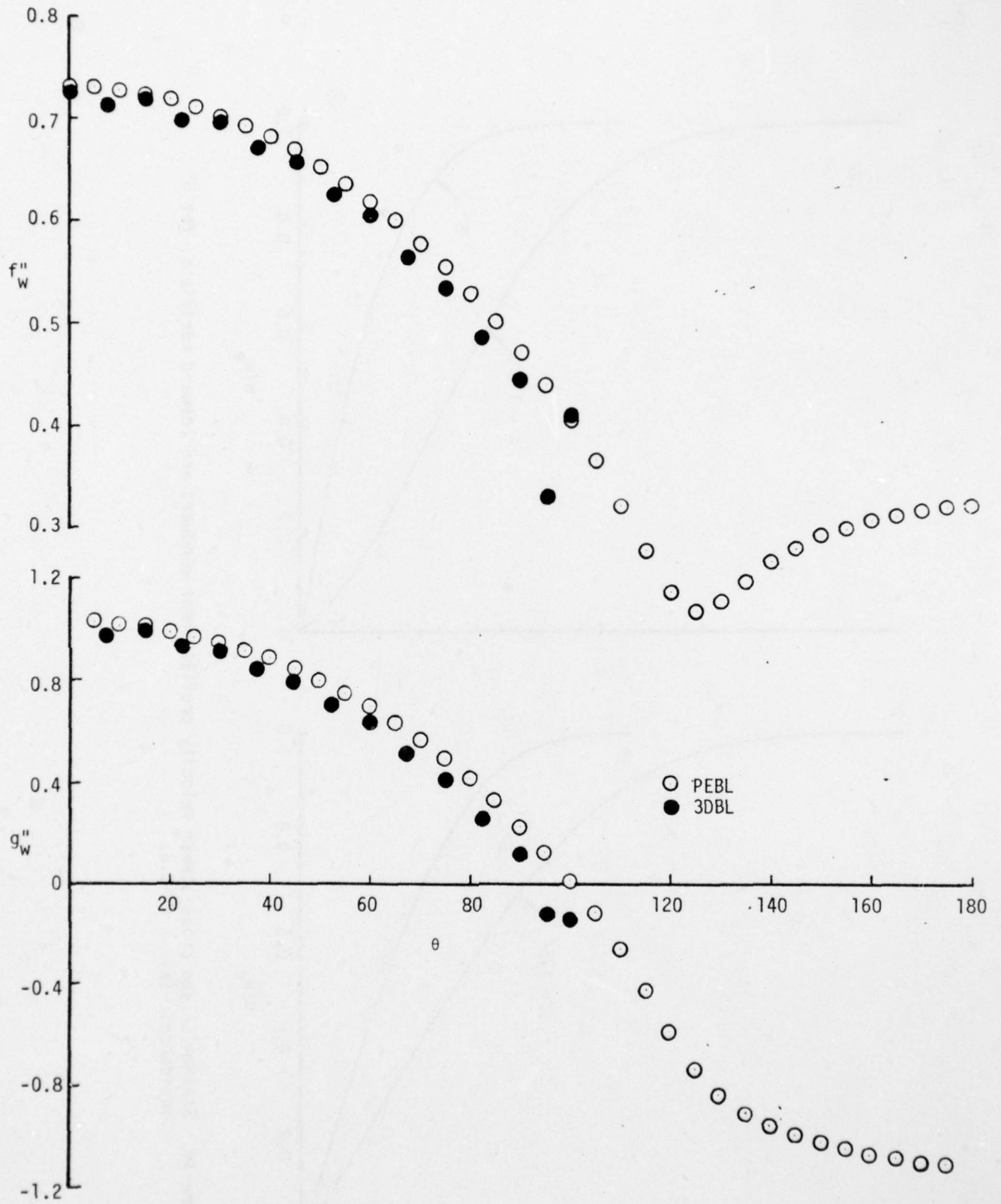
Figure 13. Continued (c) x = 0.3.

47
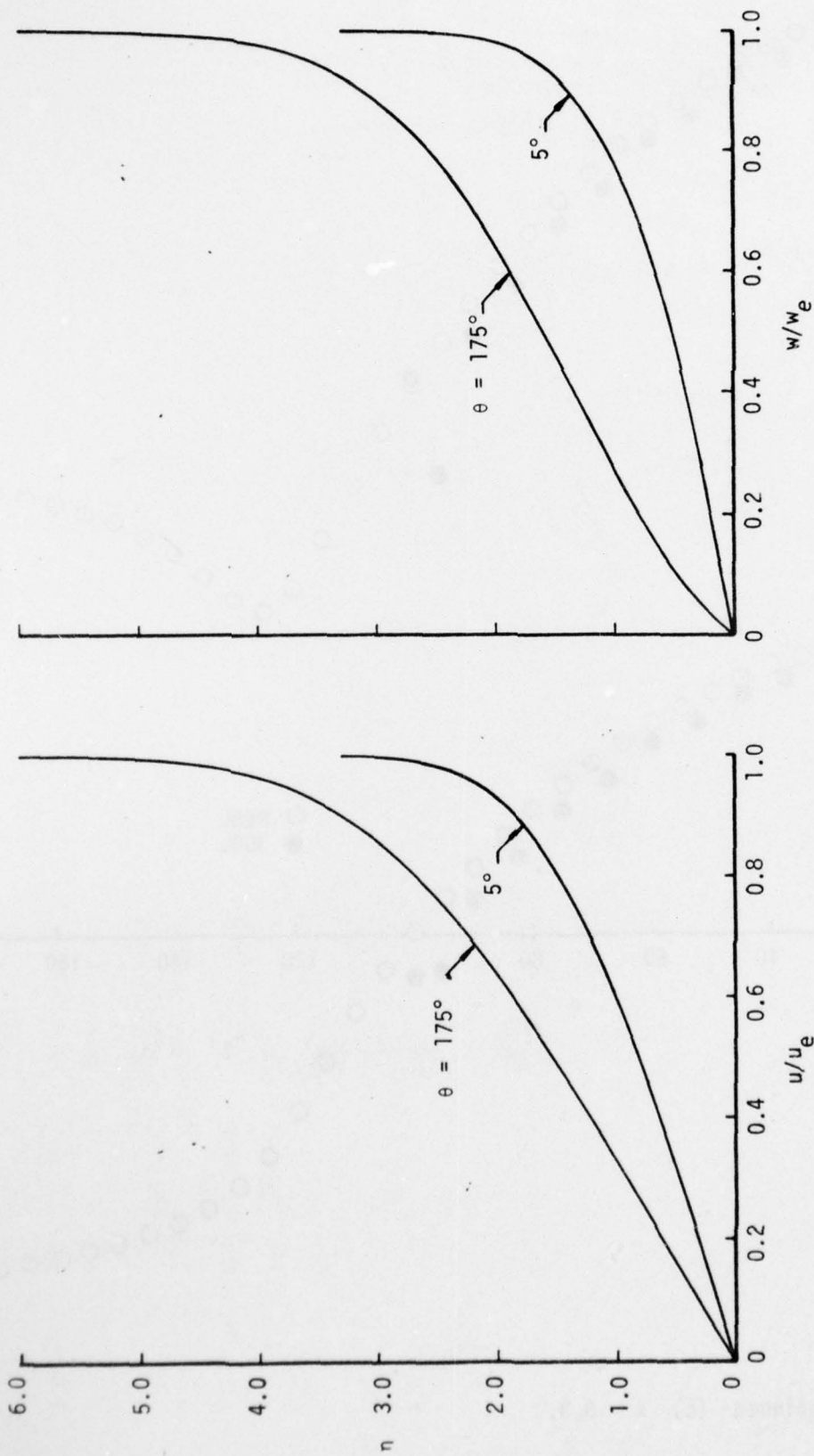
Figure 14. Streamwise and cross-stream velocity profiles near windward and leeward meridians, for 6° incidence; (a) x = -0.3.
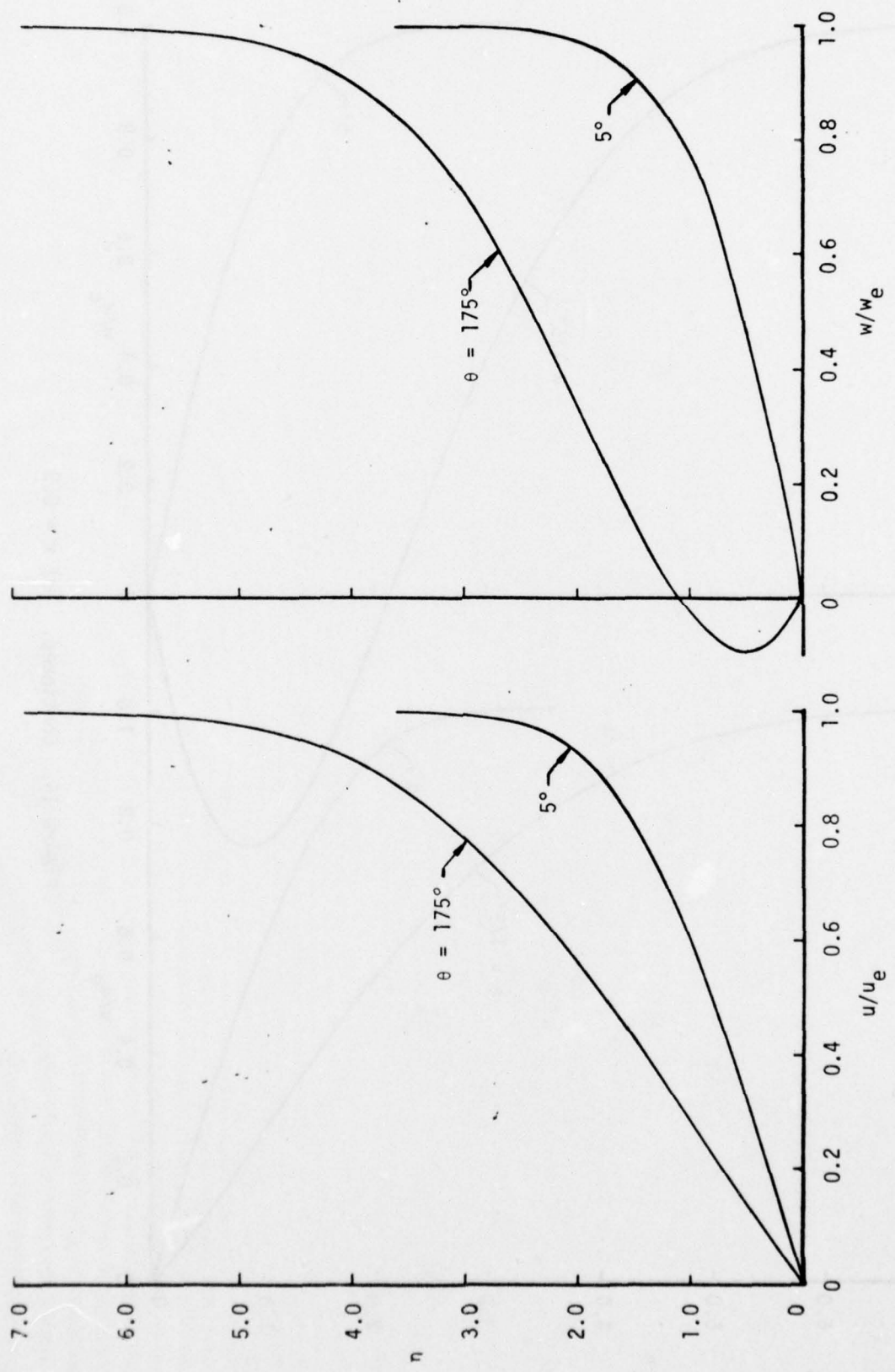
Figure 14. Continued.   (b)   x = 0.

49
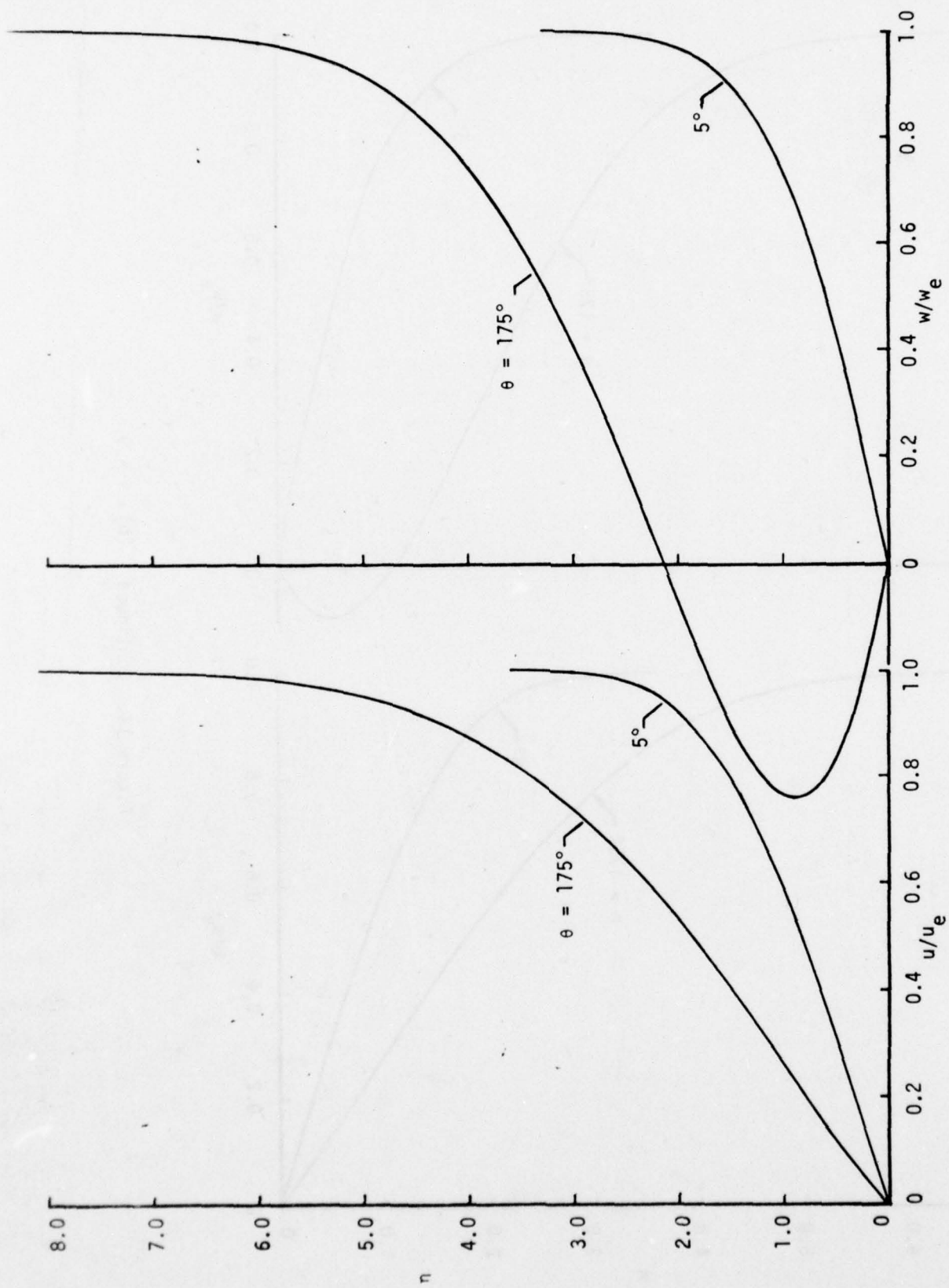
Figure 14. Continued. (c) x = 0.3

50

changed hardly at all. By the time x = 0.3 has been reached, the reverse flow layer on the lee side occupies a considerable portion of the boundary layer which has again increased significantly in thickness. There is some slight difference in the u profiles between x = 0 and x = 0.3, but the major alteration has been in w. Again, on the windward plane, except for a slight increase in thickness, both profiles are relatively unchanged.

One of the conclusions reached by Wang from his calculations, was that there was no evidence of vortical flow on the lee side of the body as the flow approached separation. It was thought that this might have been due to the use of the boundary-layer equations themselves and not truly representative of the flow field. The PEBL procedure has already been demonstrated as being capable of capturing a vortex in this sort of flow by Lin & Rubin [10],[11] and in some unpublished work at Douglas, so it was felt that the PEBL calculation might possibly yield a vortical pattern in the crossflow. The computed crossflow pattern at x = 0.3 is given in Fig. 15. Although the crossflow does exhibit reversals in direction, there is no evidence for the presence of a vortex. In fact, our results are remarkably similar to the crossflow pattern given by Wang's Fig. 8[14], and, therefore, confirm his conclusions about the lack of a vortex.

We have shown that a comparison of the 3DBL and PEBL calculation procedures produces the same results when the 3DBL method is stable. However, using the differencing given in Section 5.1, the 3DBL calculation becomes unreliable when w < 0, in agreement with predictions of stability calculations. The PEBL procedure is unconditionally stable and encounters no such difficulties. Qualitative agreement with the computed results of Wang has been shown in all cases.

The deficiency of the 3DBL method used here can be overcome by changing the differencing to the zig-zag scheme of Krause [28], which is precisely what Wang used for his calculations. The simple box scheme was used here to elucidate its behavior under adverse conditions. We are presently investigating two alternate schemes, besides the zig-zag for calculating in regions of reverse cross flow. The inability of the PEBL procedure to calculate beyond the first encountered point of separation will need further study.
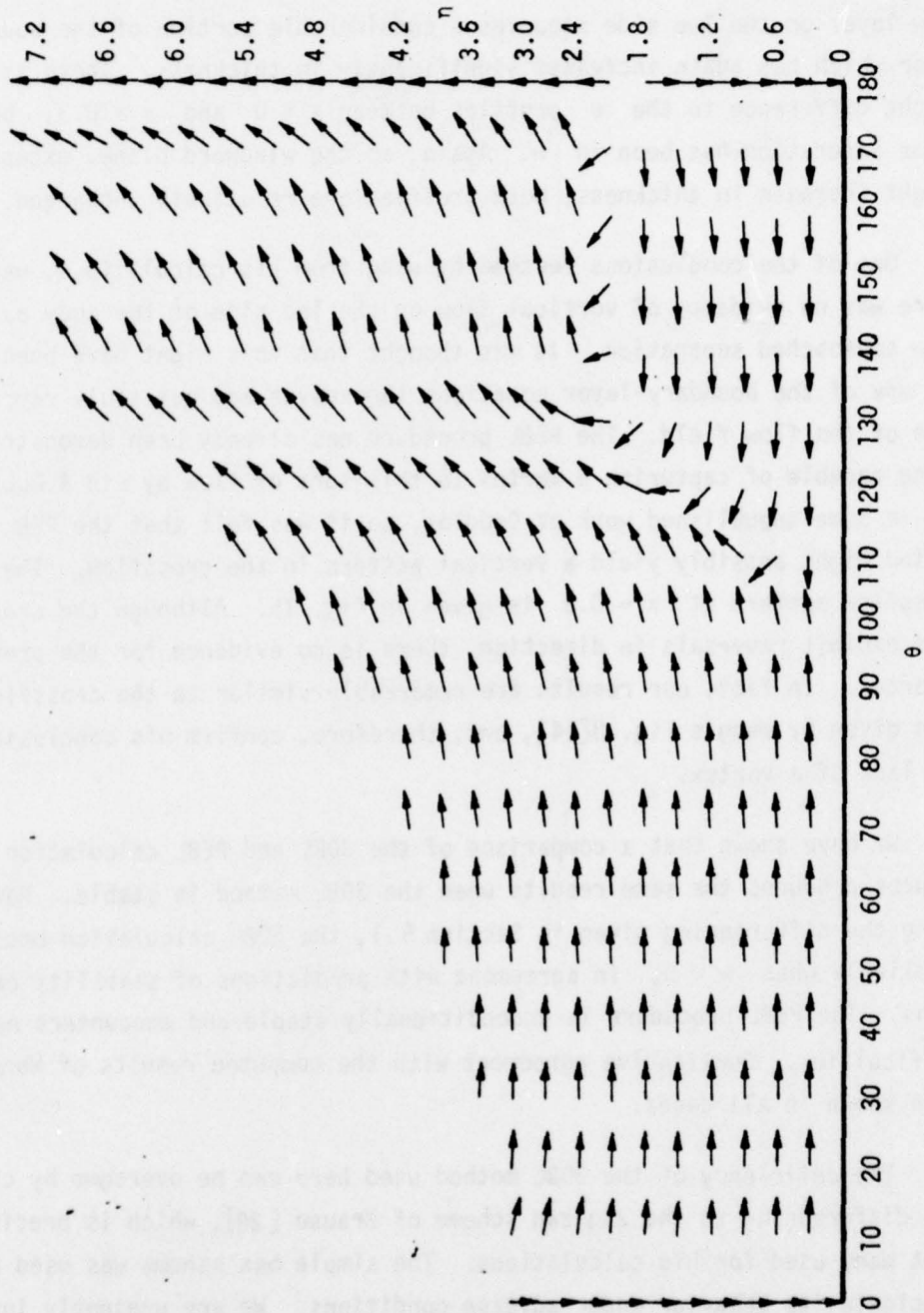
Perhaps an adaption of one of the inverse methods used in two-dimensional boundary-layer separation studies may be applicable to the PEBL procedure.

Until the initial separation point, however, it seems that the PEBL procedure and a three-dimensional procedure similar to Wang's boundary layer give comparable results. Thus, it might be assumed that the methods are interchangeable. However, this is not the case. The zig-zag differencing is only conditionally stable [28], and it is possible that regions of severe crossflow might create instabilities and make the procedure invalid. Related behavior is found when considering the flow past conical bodies. Calculations by similarity variables (to be shown in the next section) cannot progress further around the cone than the position of crossflow reversal. If the flow is not assumed to be conically similar, and is marched down the cone, as well as around in the θ direction, the situation is not altered, i.e., an integration of the standard boundary-layer equations fails at the crossflow reversal point [29]. Thus, bodies like blunted cones and elliptic cones cannot be completely described except by using the PEBL equations. In fact, the argument about whether the lee symmetry plane boundary layer can be computed independently of the rest of the flow on the body, has not been settled in any general way for bodies other than sharp circular cones [29]. For all cases, when the inflow from the body to the lee plane makes the independent symmetry plane calculation invalid, the use of the PEBL equations is required.

5.2 Conical Flow

We have used the numerical method of Section 4.1 and the eddy-viscosity formulation of Section 2.4 to obtain a solution of the system of equations for conical flow given by (3.2.4) to (3.2.6) and (3.2.11) to (3.2.13) subject to (3.2.14). Figure 16 shows a comparison of calculated and experimental results for the data of Rainbird [30], which is for a 12.5-degree half-angle cone at an angle of attack of 15.78 degrees in a supersonic stream with free-stream Mach number 1.8. The Reynolds number of the cone, based on its axial length, was 25×10^6, which indicates that the possible effect of flow nonuniformities caused by variable transition location upon the measurements at 0.85L can be neglected.

The computed results shown in Figure 16 were made by using both the "old" and the "new" procedures. According to the comparison of results with experiment, we observe that the results obtained with the new procedure give better

53
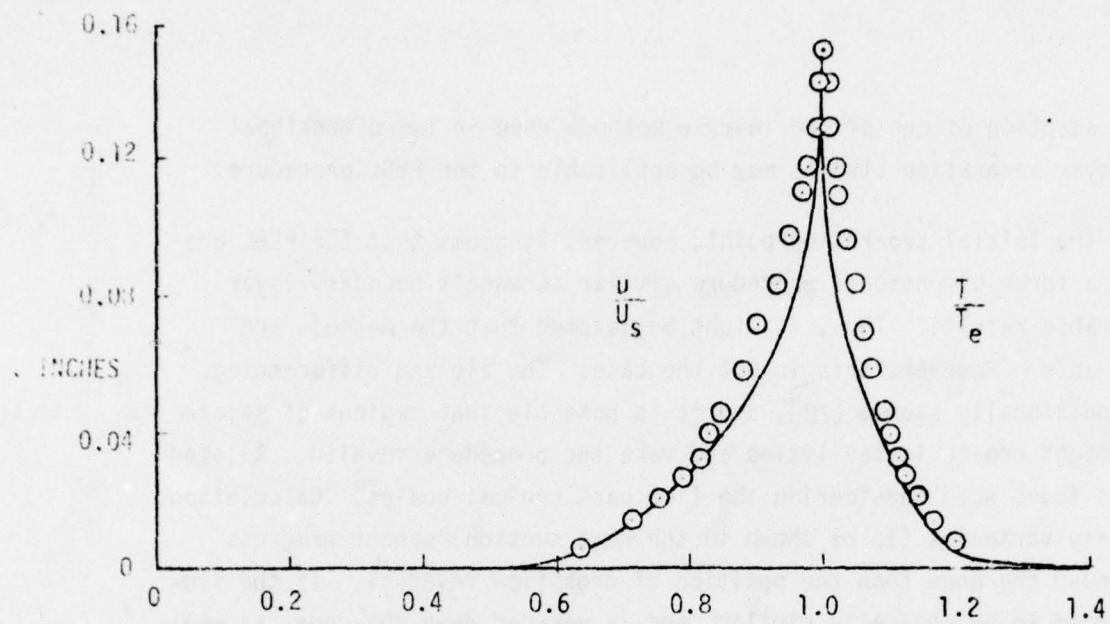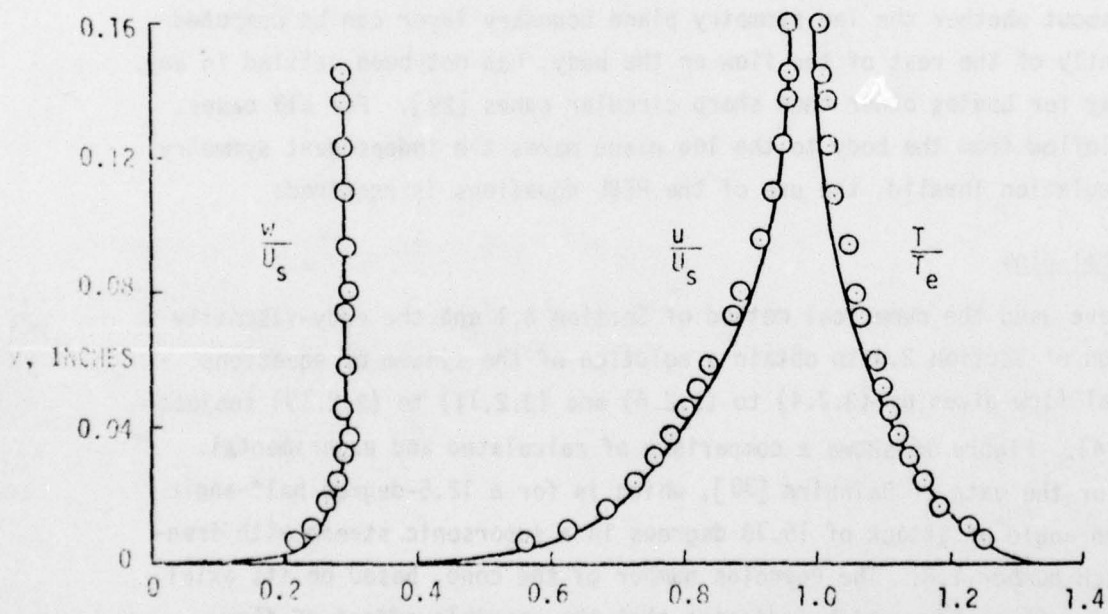
Figure 16. Comparison of measured and calculated turbulent velocity and temperature profiles for the data of Rainbird [30]. Data at 0.85 x/L from the core tip for: (a) φ = 0°, (b) φ = 45°, (c) φ = 90°, and (d) φ = 135°. Dashed lines denote calculations where the "old" procedure differs from the present one.

Figure 16. Continued.

55

Figure 16. Continued.

56
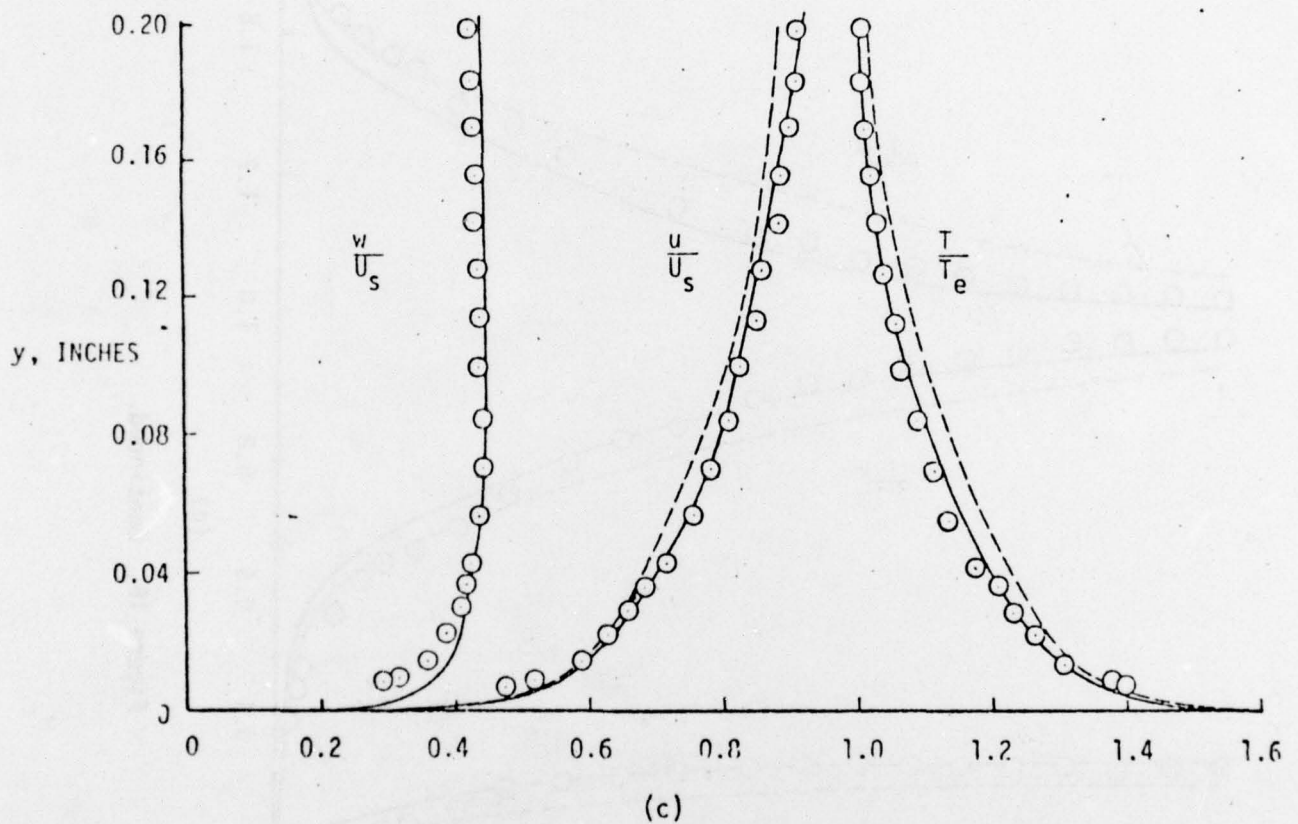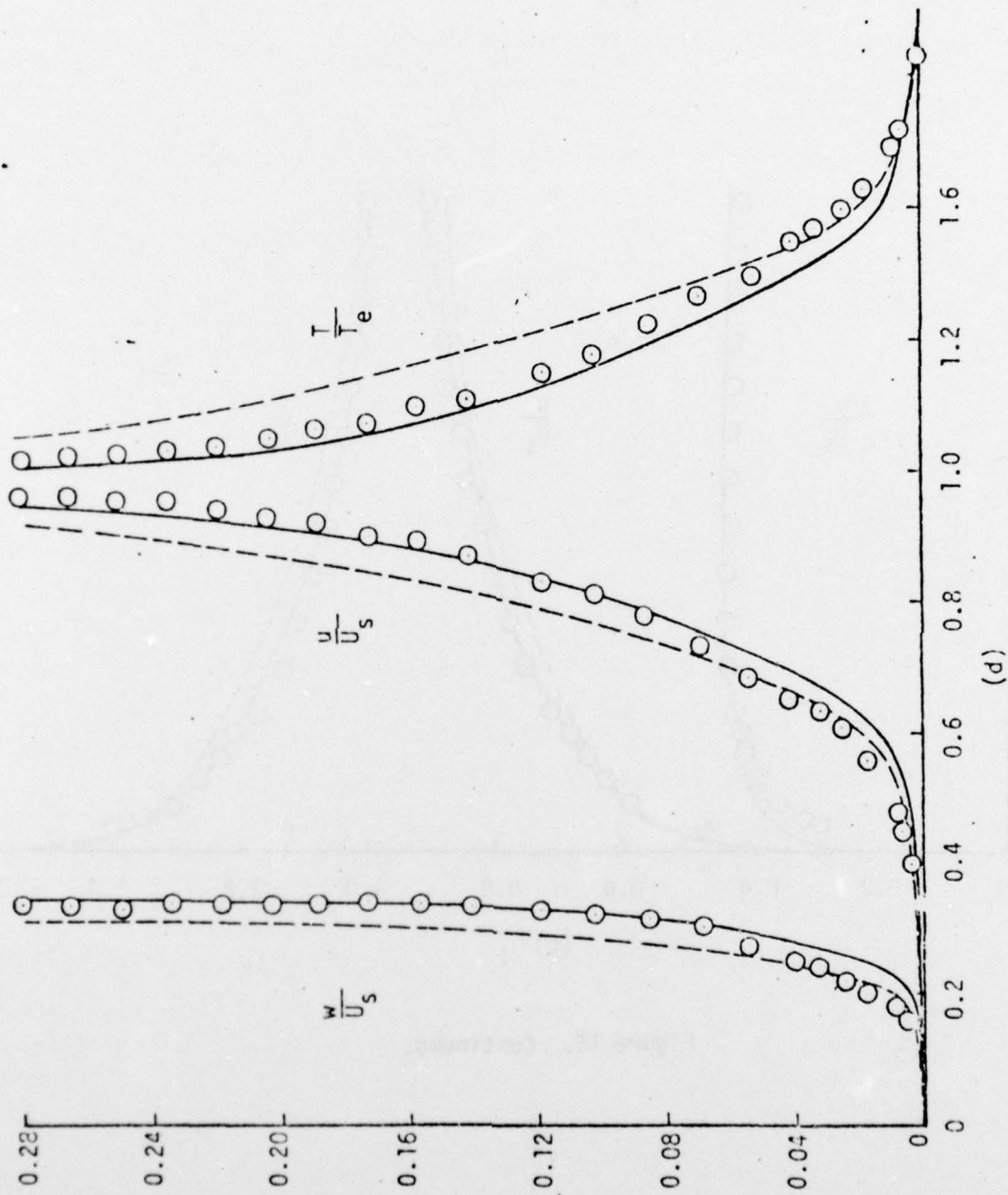
agreement with experiment than the old procedure. For circumferential angles $\phi = 0$ and $45°$ (see Figs. 16a and 16b), however, there is very little difference between the computed results obtained by either procedure; as ϕ increases, so does the difference as shown in Figs. 16c and 16d.

A note should be made of the discrepancies in the temperature and velocity profiles at $\phi = 135°$. Because of the relatively high angle of attack, the flow beyond about $\phi = 120°$ is subject to an adverse pressure gradient, which eventually leads to separation defined by zero shear stress component normal to the generator. Although our calculations with either procedure predict separation at about $\phi = 161°$, close to the measured value of $\phi = 159°$, the measured boundary layer shows a more rapid thickening than is predicted by calculations. This can be traced to vortex formation, in which case the ordinary boundary-layer equations are no longer valid anyway.

We conclude that the similarity variable proposed by Bradshaw for turbulent flows over tapered wings is also applicable to the calculation of high Reynolds number turbulent boundary layer on cones at incidence with local similarity assumptions.

Although the improvements obtained by the "new" procedure may seem small in comparison with the empiricism contained in eddy-viscosity laws and viscous/inviscid interaction effects, they are nevertheless encouraging that the local similarity will work for other similar shapes as well. In principle, the procedure is strictly applicable to conical bodies with arbitrary cross-section provided that the radial pressure gradient is very small.

57

VI. REFERENCES

1. Cebeci, T., Kaups, K., and Ramsey, J.A.: A General Method for Calculating Three-Dimensional Compressible Laminar and Turbulent Boundary Layers on Arbitrary Wings. NASA CR-2777 (1977).

2. McLean, J.D.: Three-Dimensional Turbulent Boundary-Layer Calculations for Swept Wings. AIAA Paper No. 77-3 (1977).

3. Kordulla, W.: Investigations Related to the Inviscid-Viscous Interaction in Transonic Flows about Finite Three-Dimensional Wings. AIAA Paper No. 77-209 (1977).

4. Bradshaw, P., Mizner, C.A., and Unsworth, K.: Calculation of Compressible Turbulent Boundary Layers on Straight Tapered Swept Wings. AIAA J., 14, 399-400 (1976).

5. Moore, F.K.: Laminar Boundary Layer on Cones in Supersonic Flow at Large Angle of Attack. NACA TN 2844 (1952).

6. Cooke, J.C.: Supersonic Laminar Boundary Layer on Cones. Report No. 66347, RAE, Farnborough (1965).

7. Boericke, R.R.: The Laminar Boundary Layer on a Cone at Incidence in Supersonic Flow. AIAA J., 9, 462-468 (1971).

8. Dwyer, H.A. and Sanders, B.R.: A Physically Optimum Difference Scheme for Three-Dimensional Boundary Layers. In Proceedings of the Fourth International Conference on Numerical Methods in Fluid Dynamics, 144-150, Springer-Verlag (1975).

9. Kitchens, C.W., Sedney, R., and Gerber, N.: The Role of the Zone of Dependence Concept in Three-Dimensional Boundary-Layer Calculations. In Proceedings of the AIAA 2nd Computational Fluid Dynamics Conference, 102-112 (1975)

10. Lin, T.C. and Rubin, S.G.: Viscous Flow Over a Cone at Incidence. II - Supersonic Boundary Layer. JFM, 59, 593-620 (1973).

11. Lin, T.C. and Rubin, S.G.: Viscous Flow Over Spinning Cones at Angle of Attack. Proceedings of the AIAA Computational Fluid Dynamics Conference, 51-62 (1973).

12. Wang, K.C.: Three-Dimensional Boundary Lyaer Near the Plane of Symmetry of a Sperhoid at Incidence. JFM, 43, 187-209 (1970).

13. Wang, K.C.: Boundary Layer Over a Blunt Body at High Incidence with an Open-Type of Separation. Proc. Roy. Soc., London, A340, 33-55 (1974).

14. Wang, K.C.: Boundary Layer Over a Blunt Body at Low Incidence with Circumferential Reversed Flow. JFM, 72, 49-65 (1975).

15. Roux, B.: Supersonic Laminar Boundary Layer Near the Plane of Symmetry of a Cone at Incidence. JFM, 51, 1-14 (1972).

16. Murdock, J.W.: The Solution of Sharp-Cone Boundary-Layer Equations in the Plane of Symmetry. JFM, 54, 665-678 (1972).

17. Kaups, K., and Cebeci, T.: On the Prediction of Turbulent Boundary Layers on Cones at Incidence. To be published in Journal of Aircraft (1977).

18. Cebeci, T.: Calculation of Three-Dimensional Boundary Layers. I. Swept Infinite Cylinders and Small Cross Flow. AIAA J., 12, 779-786 (1974).

19. Cebeci, T.: Calculation of Three-Dimensional Boundary Layers. II. Three-Dimensional Flows in Cartesian Coordinates. AIAA J., 13, 1056-1064 (1975).

20. Blottner, F.G., and Ellis, M.A.: Finite-Difference Solution of the Incompressible Three-Dimensional Boundary-Layer Equations for a Blunt Body. Computers and Fluids, 1, 133-158 (1973).

21. Cebeci, T. and Smith, A.M.O.: Analysis of Turbulent Boundary Layers. Academic Press, New York (1974).

22. Isaacson, E. and Keller, H.B.: Analysis of Numerical Methods. Wiley, New York (1966).

23. Hirsh, R.S.: Numerical Calculation of Supersonic Three-Dimensional Free Mixing Flows Using the Parabolic-Elliptic Navier-Stokes Equations. NASA TN D-8195 (1976).

24. Peaceman, D.W. and Rachford, H.H., Jr.: The Numerical Solution of Parabolic and Elliptic Differential Equations. J. Soc. Ind. & Appl. Math., 3, 28-41 (1955).

25. Hirsh, R.S.: An Edge Corrected Linearization Technique for Boundary Layer Problems. To be published in AIAA J. (1977).

26. Faulkner, S.M., Hess, J.L, Smith, A.M.O., and Liebeck, R.H.: Charts and Formulas for Estimating Velocity Fields in Incompressible Flow. Douglas Aircraft Company Rept. No. LB 32707 (1968).

27. Chang, K.C.: Calculation of Three-Dimensional Boundary Layers on Ship Forms. Ph.D. Thesis, University of Iowa (1975).

28. Krause, E.: Comment on Solution of a Three-Dimensional Boundary-Layer Flow with Separation. AIAA J., 7, 575-576 (1969).

29. Rubin, S.G., Lin, T.C. and Tarulli, F.: Symmetry Plane Viscous Layer on a Sharp Cone. AIAA J., 15, 204-211 (1977).

30. Rainbird, W.J.: Turbulent Boundary-Layer Growth and Separation on a Yawed Cone. AIAA J., 6, 2140-2146 (1968).

APPENDIX A

THE PARABOLIC-ELLIPTIC BOUNDARY-LAYER EQUATIONS

The standard three-dimensional boundary-layer equations have a wide range of applicability. However, when there is a region where the velocity changes rapidly in the crossflow direction, a straight-forward integration of the equations sometimes breaks down. At this point it is necessary to reexamine some of the approximations that led to the boundary-layer equations to see if any have become invalid. The major assumption in boundary-layer theory concerns the relative size of gradients of the flow quantities. That is, gradients in one direction are assumed larger than gradients in the other two directions. However, some flows do not fit within the realm of boundary-layer theory, so less stringent assumptions must be placed on the Navier-Stokes (NS) equations. Flows of this type are corner flows [A1], flows past finite width flat plates [A2], rectangular jet flows [23], [A3], flows past bodies at moderate incidence [10], [11], [A4], and, as pointed out in reference 23, wing-tip flows. In these flows, gradients in a second direction can become important, and must be accounted for.

It is possible to make a distinction among these flows which lie somewhere between simple boundary layers and solutions to the complete NS equations. In some cases it is essential that the pressure field be calculated as an integral part of the solution method. Effectively, this states that the scale lengths in the gradient directions are nearly equal. This leads to the parabolic-elliptic Navier-Stokes (PENS) equations used by references 23, A1-A4. However, there are certain circumstances where the pressure may still be presumed given by an inviscid flow calculation. This implies that the gradient in the direction of the presumed boundary layer is still the dominant factor, and the inclusion of a second direction only corrects the flow field locally. This leads to the parabolic-elliptic boundary-layer (PEBL) equations used by references 10, 11, and in this report.

The PEBL equations can be derived for the case of laminar incompressible flow past an arbitrary body of revolution by considering the Navier-Stokes equations in the general body-oriented coordinate system discussed in Section II. Reducing the general orthogonal equations given in reference A5 using the fact that $h_1 = h_1(x,\theta)$, $h_2 = h_2(x,\theta)$, $h_3 = 1$, yields after considerable algebra

60

Continuity

$$\frac{1}{h_1} u_x - K_2 u + \frac{1}{h_2} w_\theta - K_1 w + v_y = 0 \tag{A.1}$$

x-Momentum

$$\frac{1}{h_1} u u_x + \frac{1}{h_2} w u_\theta + v u_y - K_1 uw + K_2 w^2 = -\frac{1}{\rho} \frac{1}{h_1} p_x + \nu \tau_x \tag{A.2a}$$

$$\tau_x = \frac{1}{h_1^2} u_{xx} + \frac{1}{h_1} (K_{1i} - K_2) u_x + \frac{1}{h_2^2} u_{\theta\theta} - \frac{1}{h_2} (K_1 - K_{22}) u_\theta + u_{yy}$$

$$- \left(2K_2^2 + 2K_1^2 - \frac{1}{h_2} K_{1_\theta} - \frac{1}{h_1} K_{2_x} \right) u + \left(K_2 K_{22} - K_2^2 - \frac{1}{h_1} K_{1_x} + \frac{1}{h_2} K_{2_\theta} \right) w$$

$$+ 2 \left(\frac{1}{h_2} K_2 w_\theta - \frac{1}{h_1} K_1 w_x \right) \tag{A.2b}$$

θ-Momentum

$$\frac{1}{h_1} u w_x + \frac{1}{h_2} w w_\theta + v w_y - K_2 uw + K_1 u^2 = -\frac{1}{\rho} \frac{1}{h_2} p_\theta + \nu \tau_\theta \tag{A.3a}$$

$$\tau_\theta = \frac{1}{h_1^2} w_{xx} + \frac{1}{h_1} (K_{11} - K_2) w_x + \frac{1}{h_2^2} w_{\theta\theta} + \frac{1}{h_2} (K_{22} - K_1) w_\theta + w_{yy}$$

$$- \left(2K_2^2 + 2K_1^2 - \frac{1}{h_1} K_{2_x} - \frac{1}{h_2} K_{1_\theta} \right) w + \left(K_2^2 - K_2 K_{22} - \frac{1}{h_2} K_{2_\theta} + \frac{1}{h_1} K_{1_x} \right) u$$

$$+ 2 \left(\frac{1}{h_1} K_1 u_x - \frac{1}{h_2} K_2 u_\theta \right) \tag{A.3b}$$

y-Momentum

$$\frac{1}{h_1} u v_x + \frac{1}{h_2} w v_\theta + v v_y = -\frac{1}{\rho} p_y + \nu \tau_y \tag{A.4a}$$

$$\tau_y = \frac{1}{h_1^2} v_{xx} + \frac{1}{h_1} (K_{11} - K_2) v_x + \frac{1}{h_2^2} v_{\theta\theta} + \frac{1}{h_2} (K_{22} - K_1) v_\theta + v_{yy} \tag{A.4b}$$

where K_1 and K_2 are as defined by (3.1.4b) and

$$K_{11} = -\frac{1}{h_1^2} \frac{\partial h_1}{\partial x} \qquad\qquad K_{22} = -\frac{1}{h_2^2} \frac{\partial h_2}{\partial \theta}$$

61

These are the complete Navier-Stokes equations for the body-oriented coordinate system, no approximations have been made.

The three momentum equations will now be nondimensionalized in order to more easily determine the order of magnitude of the various terms in the equations. The procedure is the same as is used in standard boundary-layer theory but with one important difference. This appears in the treatment of the cross-flow velocity, w, and the derivatives in the cross plane, $\partial/\partial\theta$. The following nondimensional quantities are defined.

$$\bar{u} = \frac{u}{u_r} \quad , \quad \bar{v} = \frac{v}{\delta u_r} \quad , \quad \bar{\mu} = \frac{\mu}{\mu_r}$$

$$\bar{x} = \frac{x}{L_r} \quad , \quad \bar{y} = \frac{y}{\delta L_r} \tag{A.5a}$$

$$\bar{p} = \frac{p}{q_r} \quad , \quad \bar{\rho} = \frac{\rho}{\rho_r}$$

These are standard for boundary-layer theory where gradients in the z-direction are larger than those in the x-direction, i.e., $\delta \ll 1$. The subscript r refers to a suitable reference, and q_r is $\rho_r u_r^2$ for incompressible flow. The only change from the standard procedure, since gradients in the cross plane are being considered to possibly be large, will be to flag the cross-plane gradients with a parameter ϵ as follows:

$$\bar{\theta} = \frac{\theta}{\epsilon} \quad , \quad \bar{h} = \frac{h}{L_r} \tag{A.5b}$$

and so we must also have

$$\bar{w} = \frac{w}{\epsilon u_r} \tag{A.5c}$$

Here ϵ represents simply a means of keeping track of θ-derivatives. The value of this artifice will appear shortly when the nondimensional equations are displayed.

Placing the nondimensional variables (A.5) into the continuity and momentum equations, (A.1) - (A.4), rearranging terms, and dropping the bar denoting a nondimensional quantity, one obtains

62

Continuity

$$\frac{1}{h_1} u_x - K_2 u + \frac{1}{h_2} w_\theta - \varepsilon K_1 w + v_y = 0 \tag{A.6}$$

x-Momentum

$$\frac{1}{h_1} uu_x + \frac{1}{h_2} wu_\theta + vu_y - \varepsilon K_1 uw + \varepsilon^2 K_2 w^2 = -\frac{1}{h_1} p_x + \frac{\nu}{u_r L_r} \frac{1}{\delta^2} \tau_x \tag{A.7a}$$

$$\tau_x = u_{yy} + \frac{\delta^2}{\varepsilon^2} \frac{1}{h_2^2} u_{\theta\theta} + \frac{\delta^2}{\varepsilon} \frac{1}{h_2} (K_{22} - K_1) u_\theta$$

$$+ \delta^2 \left[\frac{1}{h_1^2} u_{xx} + \frac{1}{h_1} (K_{11} - K_2) u_x - \left(2K_2^2 + 2K_1^2 - \frac{1}{h_2} K_{1_\theta} - \frac{1}{h_1} K_{2_x} \right) u \right.$$

$$\left. - 2 \left(\frac{1}{h_1} K_1 w_x - \frac{1}{h_2} K_2 w_\theta \right) + \left(K_2 K_{22} - K_2^2 - \frac{1}{h_1} K_{1_x} + \frac{1}{h_2} K_{2_\theta} \right) w \right] \tag{A.7b}$$

θ-Momentum

$$\frac{1}{h_1} uw_x + \frac{1}{h_2} ww_\theta + vw_y - K_2 uw + \frac{1}{\varepsilon} K_1 u^2 = -\frac{1}{\varepsilon^2} \frac{1}{h_2} p_\theta + \frac{\nu}{u_r L_r} \frac{1}{\delta^2} \tau_\theta \tag{A.8a}$$

$$\tau_\theta = w_{yy} + \frac{\delta^2}{\varepsilon^2} \left(\frac{1}{h_2^2} w_{\theta\theta} - 2 \frac{1}{h_2} K_2 u_\theta \right) + \frac{\delta^2}{\varepsilon} \left[\frac{1}{h_2} (K_{22} - K_1) w_\theta \right.$$

$$\left. + \left(K_2^2 - K_2 K_{22} - \frac{1}{h_2} K_{2_\theta} + \frac{1}{h_1} K_{1_x} \right) u + 2 \frac{1}{h_1} K_1 u_x \right] + \delta^2 \left[\frac{1}{h_1^2} w_{xx} \right.$$

$$\left. - \frac{1}{h_1} (K_{11} - K_2) w_x - \left(2K_2^2 + 2K_1^2 - \frac{1}{h_2} K_{1_\theta} \right) w \right] \tag{A.8b}$$

y-Momentum

$$\frac{1}{h_1} uv_x + \frac{1}{h_2} wv_\theta + vv_y = \frac{1}{\rho} \frac{1}{\delta^2} p_y + \frac{\nu}{u_r L_r} \frac{1}{\delta^2} \tau_y \tag{A.9a}$$

$$\tau_y = v_{yy} + \frac{\delta^2}{\varepsilon^2} \frac{1}{h_2^2} v_{\theta\theta} + \frac{\delta^2}{\varepsilon} \frac{1}{h_2} (K_{22} - K_1) v_\theta + \delta^2 \left[v_{xx} + \frac{1}{h_1} (K_{11} - K_2) v_x \right]$$

$$\tag{A.9b}$$

63

Following the standard procedure of boundary-layer thoery, we now choose our y-scale such that

$$\delta^2 = \frac{\nu}{u_r L_r} = \frac{1}{R} \tag{A.10}$$

Up to this point, only the inclusion of the ε flag distinguishes this development from that of ordinary boundary-layer theory. If we were to set $\varepsilon = 1$ and then drop terms of $O(\delta)$ or higher, the standard three-dimensional boundary-layer (3DBL) equations result. However, it is just these equations we are trying to modify. They are to be modified due to phenomena in the cross plane which may cause the θ-gradients to become larger than unit order. The terms affected by these gradients can be identified by the terms flagged with an ε. The largest of these terms in (A.7) through (A.9) is of order δ^2/ε^2 in each equation. It is these extra terms we wish to keep in addition to the three-dimensional boundary-layer terms.

The behavior of the extra gradients will not be uniform throughout the flow field, so we cannot set one scale for ε as we did for δ. For example, near the windward generator on a cone no additional terms are necessary to describe the symmetry line flow other than the 3DBL equations; hence, $\varepsilon \sim O(1)$. However, near the lee meridian at moderate angles of attack, account must be taken of the inflow to the symmetry line, and so a reasonable guess is that here, in this boundary region, $\varepsilon \sim O(\delta)$. Thus, the procedure followed in keeping the significant terms in (A.7) through (A.9) is to keep all terms of $O(1)$ and $O(\delta^2/\varepsilon^2)$. All other terms are omitted. After this has been done, having identified the terms necessary to account for cross-flow effects, ε is set equal to one since its true scaling is unknown. The resulting equations contain terms which are of no importance when ε is truly order one (hence their inclusion does not alter the flow structure), but it is just these terms which will make a contribution in high θ-gradient regions. Following this procedure in equations (A.6) through (A.9) yields the following set of parabolic-elliptic boundary-layer (PEBL) equations, where the definition of δ, (A.10), has been used.

64

Continuity

$$\frac{1}{h_1} u_x - K_2 u + \frac{1}{h_2} w_\theta - K_1 w + v_y = 0 \qquad (A.11)$$

x-Momentum

$$\frac{1}{h_1} uu_x + \frac{1}{h_2} wu_\theta + vu_y - K_1 uw + K_2 w^2 = -\frac{1}{h_1} p_x + u_{yy} + \frac{1}{R} \frac{1}{h_2^2} u_{\theta\theta} \qquad (A.12)$$

θ-Momentum

$$\frac{1}{h_1} uw_x + \frac{1}{h_2} ww_\theta + vw_y - K_2 uw + K_1 u^2 = -\frac{1}{h_2} p_\theta + w_{yy} + \frac{1}{R} \left(\frac{1}{h_2^2} w_{\theta\theta} - 2 \frac{1}{h_2} K_2 u_\theta \right) .$$
$$\qquad (A.13)$$

y-Momentum

$$0 = p_y \qquad (A.14)$$

All the terms above are easily recognized. Those with no Reynolds number are the ordinary boundary-layer equations, and remaining terms multiplied by 1/R are the new ones needed to account for cross-plane phenomena. Thus, the equations are now elliptic in two directions (θ and y) but still allow a parabolic march in the x-direction. The pressure is determined from the externally determined inviscid field. This is by no means the same as having an additional equation similar to (A.13), instead of (A.14), had the scale length ε been chosen identical to δ at the outset of the analysis. This leads to the parabolic elliptic Navier-Stokes equations, used by [23], [A3]-[A4], where the computation of the pressure is an essential part of the solution. It is precisely the calculation of the pressure that makes NS calculations difficult. By choosing the PEBL scaling in suitable problems, this difficulty is overcome. This procedure has been used previously by Lin and Rubin for compressible flow past nonrotating [10] and rotating [11] cones at incidence.

References

A1. Rubin, S.G.: Incompressible Flow Along a Corner. JFM, 26, 97-110
(1966).

A2. Nardo, C.T. and Cresci, R.J.: An Alternating Direction Implicit Scheme
for Three-Dimensional Hypersonic Flows. J. Comp. Phys., 8, 268-284
(1971).

A3. McDonald, H. and Briley, W.R.: Three-Dimensional Supersonic Flow of a
Viscous or Inviscid Gas. J. Comp. Phys., 19, 150-178 (1975).

A4. Lubard, S.C. and Helliwell, W.S.: Calculation of the Flow on a Cone at
High Angle of Attack. AIAA Paper No. 73-636 (1973).

A5. Back, L.H.: Conservation Equations of a Viscous, Heat-Conducting Fluid
in Curvilinear Orthogonal Coordinates. JPL Tech. Rept. 32-1332 (1968).

REPORT DOCUMENTATION PAGE		READ INSTRUCTIONS BEFORE COMPLETING FORM
1. REPORT NUMBER	2. GOVT ACCESSION NO.	3. RECIPIENT'S CATALOG NUMBER
4. TITLE (and Subtitle) Calculation of Three-Dimensional Boundary Layers on Bodies of Revolution at Incidence		5. TYPE OF REPORT & PERIOD COVERED Final Jan. 1976 to Jan. 1978
		6. PERFORMING ORG. REPORT NUMBER
7. AUTHOR(s) Tuncer Cebeci, Richard S. Hirsh, and Kalle Kaups		8. CONTRACT OR GRANT NUMBER(s) N60921-76-C-0089
9. PERFORMING ORGANIZATION NAME AND ADDRESS McDonnell Douglas Corporation Douglas Aircraft Company 3855 Lakewood Blvd., Long Beach, CA 90846		10. PROGRAM ELEMENT, PROJECT, TASK AREA & WORK UNIT NUMBERS
11. CONTROLLING OFFICE NAME AND ADDRESS Naval Surface Weapons Center White Oak Silver Spring, Maryland 20910		12. REPORT DATE January 1978
		13. NUMBER OF PAGES 71
14. MONITORING AGENCY NAME & ADDRESS(if different from Controlling Office)		15. SECURITY CLASS. (of this report) Unclassified
		15a. DECLASSIFICATION/DOWNGRADING SCHEDULE

16. DISTRIBUTION STATEMENT (of this Report)

Approved for public release; distribution unlimited.

17. DISTRIBUTION STATEMENT (of the abstract entered in Block 20, if different from Report)

18. SUPPLEMENTARY NOTES

19. KEY WORDS (Continue on reverse side if necessary and identify by block number)
boundary layers
laminar boundary layers
turbulent boundary layers
three-dimensional boundary layers

20. ABSTRACT (Continue on reverse side if necessary and identify by block number)
The laminar three-dimensional boundary layer on a body of revolution at incidence is investigated using two methods. In the first, the standard equations are solved numerically using the Keller box scheme. The second method solves a set of equations, which contain the standard equations, derived from the assumption that crossflow gradients may be important. Since these equations are elliptic in the crossflow plane, an ADI procedure is used for their solution. In regions where there is no crossflow reversal, both methods yield

the same results. However, differences appear in regions where the crossflow is not unidirectional. Reasons for this discrepancy are discussed and the relative merits of each procedure identified.